Analysis of precipitation changes and its possible reasons in Songhua River Basin of China

Tianxiao Li, Zhaoqiang Zhou, Qiang Fu, Dong Liu, Mo Li, Renjie Hou, Wei Pei and Linqi Li

ABSTRACT

Changes in precipitation have a great influence on human beings. The study of precipitation can aid in understanding regional climate change characteristics and the hydrological cycle. Therefore, in this study, the standardized precipitation index is combined with a simple linear regression test, Mann–Kendall trend analysis, Sen's slope method, principal component analysis and partial correlation analysis to study precipitation and drought distributions in the Songhua River Basin and the causes of precipitation changes in this area. The results are as follows: (1) The average annual precipitation change in this area is not significant, but there are significant differences in seasonal precipitation changes. (2) On a long-term time scale, this area presents a wet trend from southeast to northwest. On a short-term time scale, spring and winter show a wet trend. Winter has changed significantly. Summer and autumn show a dry trend. (3) The average annual and rainy season (RS) precipitation shows step change characteristics. Precipitation change in RS is the main reason for annual precipitation change. (4) The Asian meridional circulation/zonal index have significant effects on precipitation and dry/wet changes in this area. The western Pacific subtropical high and the East Asian summer monsoon are also important factors in this area.

Key words | atmospheric circulation index, average annual precipitation, monthly average precipitation, Songhua River Basin, standardized precipitation index

Tianxiao Li
Zhaoqiang Zhou
Qiang Fu (corresponding author)
Dong Liu
Mo Li
Renjie Hou
Wei Pei
Linqi Li
School of Water Conservancy and Civil Engineering,
Northeast Agricultural University,
Harbin, Heilongjiang 150030,
China
E-mail: *fuqiang0629@126.com*

INTRODUCTION

It is widely recognized that global warming and climate change have had an important impact on environmental variables in many parts of the world in the past century. The fourth IPCC assessment report showed that the average global annual temperature has increased by 0.74 °C over the past 100 years. Global warming has become an indisputable fact. Significant changes have taken place in water resources and hydrological cycle processes due to the impact of increasing global climate change and human activities (Jang *et al.* 2016; Levine & Boos 2016; Beamer *et al.* 2017; Fan *et al.* 2017; Mehran *et al.* 2017). Currently, the shortage of water resources has become one of the most important factors affecting national food security, ecological security, and economic and social development, which has drawn the attention of governments and experts from all over the world (Wang *et al.* 2016a, 2016b; Miah *et al.* 2017; Simonovic 2017; Voisin *et al.* 2017; Li & Fu 2019). Climate change has resulted in a change in the spatial and temporal distribution of water resources. In recent years, many experts and scholars have made use of historical precipitation observations, extreme precipitation events, and droughts and floods to analyse changing precipitation patterns.

Precipitation is an important part of the hydrological cycle and one of the most important variables reflecting climate change. Understanding the temporal and spatial changes of precipitation has far-reaching scientific and practical significance, especially for countries that mainly rely on rain-fed agriculture. Therefore, the study of precipitation

doi: 10.2166/wcc.2019.250

changes has attracted worldwide attention (Gummadi *et al.* 2017; Paparrizos *et al.* 2017; Dhakal & Tharu 2018). In China, changes in precipitation patterns are not only considered to be important climatic factors that cause changes in surface water resources but also considered important factors influencing social development. Wang *et al.* (2015) found that the change in precipitation in China was complex, precipitation changes in each region were very different, and precipitation in the east and west showed opposing trends. Zhang *et al.* (2013a, 2013b) found that the drought trend mainly occurred in the areas covered by the Yellow River Basin, Huaihe River Basin and Haihe River Basin. The change in the precipitation index in Northeast China is relatively gentle. Lu *et al.* (2014a, 2014b) used the observed precipitation and NCEP-NCAR (National Center for Environmental Prediction-National Center for Atmospheric Research) reanalysis to analyse changes in summer precipitation in China. The results showed that summer precipitation increased in the southeast and west, but decreased in the northeast. Shi *et al.* (2016) suggested that the east showed a trend of increasing precipitation in the desertification areas of China, whereas the west showed a trend of decreasing precipitation. Zhang *et al.* (2015) found that the extreme precipitation intensity increased in the Huang–Huai–Hai Basin from 1960 to 2010, but the frequency decreased. Obvious spatial differences in extreme precipitation events were observed in different climatic regions. Guo *et al.* (2016) researched the mid-western area of Liaoning Province and showed that the frequency of extreme precipitation in the Liaoning semi-arid area exhibited a significant downward trend and that the spatial distribution of extreme precipitation events was significantly different. Khan *et al.* (2016) showed an obvious increasing trend in precipitation in the Songhua River Basin (SRB) in the spring and winter and an obvious decreasing trend in the autumn. The annual precipitation distribution in the SRB is uneven. Fu *et al.* (2018a, 2018b) selected five GCM (General Circulation Model) scenarios to simulate precipitation in the Songhua River and found that precipitation in the flood season changed significantly and irregularly. In general, rainfall varies greatly by season and region in China.

In addition, analysis of the changes in drought is important. Drought is a kind of natural disaster that cannot meet the needs of human activities and the environment due to the absence of normal or expected precipitation. At present, there are many indicators to describe dry and wet events. Commonly used indicators include the Palmer drought severity index (PDSI) (Guo *et al.* 2018), the standardized evapotranspiration index (SPEI) (Ta *et al.* 2018) and the standardized precipitation index (SPI) (Güner Bacanli 2017). The data requirements for the PDSI, which is based on the soil/water balance, are relatively high. This index also lacks the flexibility to adapt to the multi-scalar nature inherent in drought. The SPEI is able to identify a link between increased drought and the need for more water to evaporate. The SPEI also has the same multi-scale characteristics as the SPI does. However, this method also has shortcomings. Since many stations in the SRB have low temperatures when the evapotranspiration is zero, the parameters are not defined, so this parameter is not suitable for the middle-high latitude cold zone. Therefore, the SPI, with its multi-scale characteristics and broad applicability, is chosen for use in this paper.

The SRB is located in the cold region of north-eastern China and is one of the seven major basins in China. This region plays an important role in the sustainable development of the ecological environment in north-eastern China. Moreover, as an important food production base in China, it also plays a vital role in food security in China. In recent years, natural disasters, such as floods, droughts and heavy rains, have frequently occurred in the cold regions of the SRB, which not only affect social and economic development but also threaten human survival. Drought has a great impact on human livelihood, agricultural production and ecosystem water use, especially in the Songnen Plain, which is dominated by rain-fed agriculture (Song & Zhao 2012). Thus, research on precipitation in the SRB has attracted increasing attention (Song *et al.* 2015a, 2015b; Faiz *et al.* 2018). However, there is no comprehensive study on the precipitation and dry/wet changes in the SRB, and there are few studies on the causes of precipitation changes in the cold region in the context of global warming. However, to the best of our knowledge, although many studies have investigated regional precipitation and dry/wet patterns, few studies have specifically studied rainfall changes in the SRB and their possible causes. Therefore, obtaining a comprehensive understanding of precipitation change is not only related to the sustainable development of water resources but also has great significance for the

management and planning of water resources, the planning of agricultural production and the prevention of drought and flood disasters in the SRB.

Therefore, this study investigated precipitation changes in the SRB, which is located in the cold region, from 1960 to 2013 and the possible reasons for these changes. The main novel findings and objectives are as follows: (1) the precipitation variation patterns of the SRB located in the cold region were analysed from multiple scales (year–season–month); (2) meteorological wet/dry conditions were analysed from multi-scales; (3) the contribution of monthly precipitation to changes in annual precipitation was quantified, and the relationship between monthly precipitation patterns and annual precipitation was clarified; and (4) possible reasons for the precipitation changes in the SRB were summarized.

RESEARCH AREA

Study area

The SRB (119°52′–132°31′E and 41°42′–51°48′N) is located in Northeast China (Figure 1). The SRB is one of China's seven major river basins, covering a total area of 556,800 km^2. The Songhua River was formed by the convergence of the second tributary of the southern Songhua River and the northern part of the Nenjiang River. The SRB is located on the northern edge of the East Asian monsoon, which results in a strongly fluctuating annual climate due to the competing influences of the East Asian monsoon and the subtropical high (Liu *et al.* 2012). The SRB is composed of three sub-basins: the northeast lower Songhua River Basin (LSRB), the upper Songhua River Basin (USRB) in the south and the Nenjiang River Basin (NRB) in the west. Because of the large geographic extent and elevation differences, the climatic and hydrologic conditions of the SRB are complex. The annual precipitation is less than 400 mm in the southwest and more than 750 mm in the east. Floods and droughts alternately occur in the basin. The annual average temperature ranges between 1 and 5 °C, and the annual amount of sunshine is between 2,200 and 3,300 h from east to west (Qi *et al.* 2013).

Data sources

Monthly precipitation data were collected from the China Meteorological Data Service Centre (CMDC). Since the

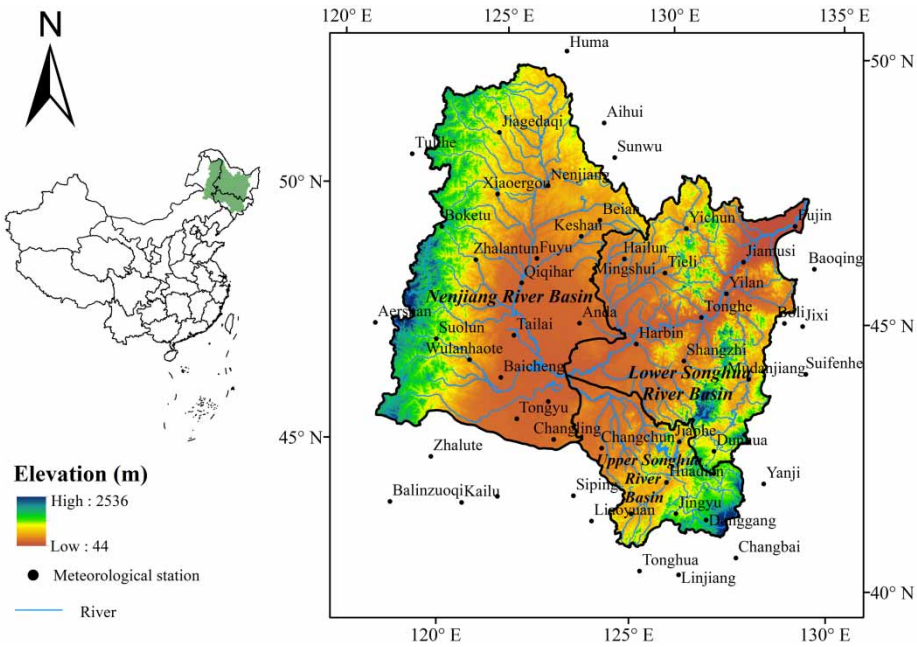

Figure 1 | Study area and meteorological station distributions.

monthly precipitation data from 1960 to 2013 were relatively complete, the precipitation observation data during this period were selected for this study. When the national meteorological stations were set up, the average spacing of the first-stage stations was approximately 100 km, and the distribution was relatively uniform. Priority was given to key and sensitive regions. Then, according to the typical spatial and temporal characteristics of the medium-scale weather system, we referred to the design of the international medium-scale ground observation network, and various factors, such as the area of each province (autonomous region or municipality directly under the central government), demand for observation elements, annual average rainfall and population density, were taken into account to increase the regional observation stations. A total of 35 weather stations (Song *et al.* 2015a, 2015b) in the SRB and 19 weather stations outside the basin were selected. The Chinese meteorological data network strictly controls the quality of data before they are released, including checking for incorrect codes and records as well as homogenizing the data. The standardized precipitation indices SPI3 and SPI24 were calculated and used to measure the spatial and temporal distributions of droughts and floods in the SRB.

Based on previous research, the western Pacific subtropical high (Guo *et al.* 2017), East Asian summer monsoon (EASM, Liang *et al.* 2015), Asian meridional/zonal circulation (Wei & Huang 2010) and Pacific decadal oscillation (PDO, She *et al.* 2016) were used to analyse the relationship between precipitation and atmospheric circulation patterns. The Western Pacific Subtropical High Intensity (WPSI) index and the Western Pacific Subtropical High Area (WPSA) index were obtained from the CMDC. The Asian Meridional/Zonal Circulation Index (AMCI/AZCI) was obtained from http://cmdp.ncc-cma.net/cn/index.htm. The PDO index was obtained from http://jisao.washington.edu. The EASM index was obtained from http://ljp.gcess.cn/dct/page/65577.

METHODOLOGY

Standardized precipitation index

The SPI was computed by including the long-term monthly precipitation data for a given period (McKee *et al.* 1993). It is well known that the SPI values on 3- and 6-month time scales are useful for detecting agricultural drought events. On longer time scales (SPI12 and SPI24), this index is more suitable for water management (Raziei *et al.* 2009; Huang *et al.* 2014; Li & Wang 2016). The 24-month time scale permits the capture of low-frequency variation while avoiding a specific annual period. This time frame has been proved to be an appropriate time scale for describing the characteristics of regional dry and wet variations (Raziei *et al.* 2009; Vergni *et al.* 2015; Wang *et al.* 2016a, 2016b). Therefore, SPI3 and SPI24 are selected in this study to analyse the characteristics of dry and wet changes on short-term and long-term time scales, respectively. The results can serve as a reference for agricultural production planning and regional water resource management.

Precipitation generally follows not only a normal distribution but also a skewed distribution. The SPI first uses a Gamma distribution to describe the precipitation and then normalizes the skewed probability distribution. Finally, the dry and wet grades are classified by the cumulative frequency distribution of standardized precipitation, as shown in Table 1. The SPI categories are based on the classification of meteorological drought promulgated by China (GB/T 20481-2017) and have been approved by domestic and foreign researchers after many years of application (Xu *et al.* 2015; Dabanli *et al.* 2017).

The specific calculation is as follows:

Assuming that x is the accumulated precipitation on a certain time scale, which follows a Gamma distribution, the probability density function is as follows:

$$g(x) = \frac{1}{\beta^{\alpha}\Gamma(\alpha)} x^{\alpha-1} \mathrm{e}^{-x/\beta}, x > 0 \quad (1)$$

Table 1 | SPI value categories

Probability (%)	SPI	Category
2.30	≥2	Extremely wet
4.40	(1.5,2]	Severely wet
9.20	(1,1.5]	Moderately wet
68.20	(−1,1]	Normal
9.20	(−1.5, − 1]	Moderately drought
4.40	(−2, − 1.5]	Severely drought
2.30	≤− 2	Extremely drought

where $\Gamma(\alpha)$ is the Gamma function, α is the shape parameter, β is the scale parameter, and x is the sum of the monthly precipitation ($x > 0$). The maximum likelihood method is used to estimate the values of parameters α and β, and then the cumulative probability of the observed precipitation events in a given month is calculated with the obtained parameters. Since the Gamma function is not defined at 0 but the precipitation may nevertheless be 0, the cumulative function becomes:

$$H(x) = q + (1 - q)G(x) \tag{2}$$

In this formula, q represents the probability that the precipitation value is 0, and $G(x)$ is the incomplete Gamma function, which represents the cumulative distribution probability of $G(x)$. By transforming $H(x)$ into a standard normal distribution function, the SPI is obtained as follows:

$$Z = \mathrm{SPI} = -\left(t - \frac{c_0 + c_1 t + c_2 t^2}{1 + d_1 t + d_2 t^2 + d_3 t^3}\right), \quad 0 < H(x) \le 0.5 \tag{3}$$

$$Z = \mathrm{SPI} = +\left(t - \frac{c_0 + c_1 t + c_2 t^2}{1 + d_1 t + d_2 t^2 + d_3 t^3}\right), \quad 0.5 < H(x) \le 1 \tag{4}$$

where

$$t = \sqrt{\ln\left(\frac{1}{(H(x))^2}\right)}, \quad 0 < H(x) \le 0.5 \tag{5}$$

$$t = \sqrt{\ln\left(\frac{1}{(1 - H(x))^2}\right)}, \quad 0.5 < H(x) \le 1 \tag{6}$$

and c_0, c_1, c_2, d_1, d_2, and d_3 are the calculation parameters whereby the Gamma distribution function is converted into the cumulative frequency to simplify the approximate solution formula; the specific values are $c_0 = 2.5155117$, $c_1 = 0.802853$, $c_2 = 0.010328$, $d_1 = 1.432788$, $d_2 = 0.189269$, and $d_3 = 0.001308$.

Mann–Kendall test

The World Meteorological Organization (WMO) recommends the use of the Mann–Kendall (MK) test to assess trends in climatology and hydrology (Burn & Taleghani 2013; Pakalidou & Karacosta 2017). The MK trend analysis method is a nonparametric statistical test method. Its advantages are that the distribution of the samples does not need to follow a certain pattern, it does not suffer from interference from a few outliers, and the calculation is simple because there is no need to perform statistical analysis. This approach has been widely applied for the evaluation of trends in precipitation over time (Abbam *et al.* 2018; Gao *et al.* 2018). For a given time series $X = \{x_1, x_2, \ldots x_n\}$, the MK rank statistic S is given by the following equation:

$$S = \sum_{i=1}^{n-1} \sum_{j=i+1}^{n} \mathrm{sgn}\,(x_j - x_i) \tag{7}$$

where

$$\mathrm{sgn}(x_j - x_i) = \begin{cases} +1 & \text{if } (x_j - x_i) > 0 \\ 0 & \text{if } (x_j - x_i) = 0 \\ -1 & \text{if } (x_j - x_i) = 0 \end{cases} \tag{8}$$

Assuming that all variables are independent and identically distributed, the statistical variable S obeys a normal distribution with a mean of 0 and a variance of:

$$\mathrm{Var}(S) = \frac{n(n-1)(2n+5) - \sum_{i=1}^{n} t_i(i-1)(2i+5)}{18} \tag{9}$$

where t is the range of any given node, and when $n > 10$, the MK statistic is calculated using the following equation:

$$Z_c = \begin{cases} \dfrac{S-1}{[\mathrm{Var}(S)]^{0.5}} & (S > 0) \\ 0 & (S = 0) \\ \dfrac{S+1}{[\mathrm{Var}(S)]^{0.5}} & (S < 0) \end{cases} \tag{10}$$

The original time series has a significant increasing or decreasing tendency if $Z_c \ge Z_{1-\alpha/2}$ or $Z_c \le Z_{1-\alpha/2}$ at the given α-confidence level. Then, the statistical index UFk can be calculated as:

$$UF_k = \frac{s_k - E(s_k)}{\sqrt{\mathrm{Var}(s_k)}} = 1, 2, \ldots, n. \tag{11}$$

where $E(s_k) = k(k-1)/4$, $\mathrm{Var}(s_k) = k(k-1)(2k+5)/72$. Another statistical index, UBk, can also be calculated

using time series $x_n, x_{n-1}, \ldots, x_2, x_1$. The intersection of UFk and UBk curves between confidence intervals is the time when the point of abrupt occurs.

Simple linear regression test method

In this study, a simple linear regression test is used to obtain the precipitation time series trend. The simple linear regression test method is widely used in trend analyses of precipitation time series (Lupikasza 2010; Hussain & Lee 2014; Sharma & Babel 2014; She *et al.* 2016) and can well reflect the quantitative relationships between the research elements. A linear relationship is determined by examining the association between the independent time variable and its corresponding dependent variable of interest. The test statistic S follows Student's t-distribution with n-2 degrees of freedom under the null hypothesis (critical test statistics for various significance levels can be obtained from Student's t statistical table) and can be obtained as follows:

$$S = b/\sigma \tag{12}$$

where b is the estimated intercept and σ is the standard error.

Sen's slope method

Sen's slope method is a nonparametric test that allows for missing values and does not require data to conform to a specific distribution. The steepness of the trend is measured through the median, and Sen's slope estimator (Sen 1968) is calculated as follows:

$$\beta = \text{Median}\left[\frac{x_j - x_k}{j-k}\right] \quad \text{for all } k < j \tag{13}$$

where $1 \le k \le j \le n$. β is a robust estimate of the trend magnitude. Positive/negative values of β represent upward/downward trends. Sen's slope method is often used to quantify changes in the MK trend analysis (Zheng *et al.* 2017; Guo *et al.* 2018; Minaei & Irannezhad 2018). Here, Sen's slope method is also used to estimate the magnitude of the trend from the MK trend analysis.

Principal component analysis

Principal component analysis (PCA) is a commonly used dimensionality reduction method for the analysis of the original features of data. This analysis is a standard statistical method that often is used in hydrology and meteorology (Huang *et al.* 2014, 2015; Lena *et al.* 2014). PCA is often used to identify climate data patterns and to emphasize similarities and differences between them. The total variance is explained by reducing the original relevant variables to several uncorrelated new variables. The new (unrelated) variables are called the principal component (or principal component score) and consist of linear combinations of the original variables. In our study, there are 35 original SPI24 series ($X_{i,1}X_{i,2}\ldots X_{i,k}$) and 35 principal components ($Y_{i,1}Y_{i,2}\ldots Y_{i,k}$), where k represents the number of meteorological stations and i represents the length of the SPI24 series. The linear relationship is as follows:

$$\begin{bmatrix} X_{i,1} \\ X_{i,2} \\ \vdots \\ X_{i,k} \end{bmatrix} \cdot \begin{bmatrix} a_{11}a_{12}\ldots a_{1k} \\ a_{21}a_{22}\ldots a_{2k} \\ \vdots \quad \vdots \quad \ldots \quad \vdots \\ a_{k1}a_{k2}\ldots a_{kk} \end{bmatrix} = \begin{bmatrix} Y_{i,1} \\ Y_{i,2} \\ \vdots \\ Y_{i,k} \end{bmatrix} \tag{14}$$

where $(X_{i,1}X_{i,2}\ldots X_{i,k})$ is the original variable matrix and the coefficients $(a_{11}a_{12}\ldots a_{kk})$ refer to loading. The Y values are the orthogonal and new linearly uncorrelated variables that explain most of the total variance (Huang *et al.* 2014). To find a more stable localized drought pattern, varimax rotations (Santos *et al.* 2010; Li & Wang 2016) were applied to the selected PCs. Varimax rotation can further maximize the variance of the squared correlations between the rotated principal components and the variables and simplify spatial patterns with similar temporal variations (Zhao *et al.* 2012a, 2012b; Huang *et al.* 2015). Varimax rotations are the most common orthogonal method for improving the creation of regions of maximum correlation between the variables and components (Bordi *et al.* 2004; Fu *et al.* 2018a, 2018b; Guo *et al.* 2018).

RESULTS AND ANALYSIS

Temporal and spatial distribution of precipitation

The amount of precipitation in China varies greatly with seasons and regions. Therefore, to better understand the characteristics

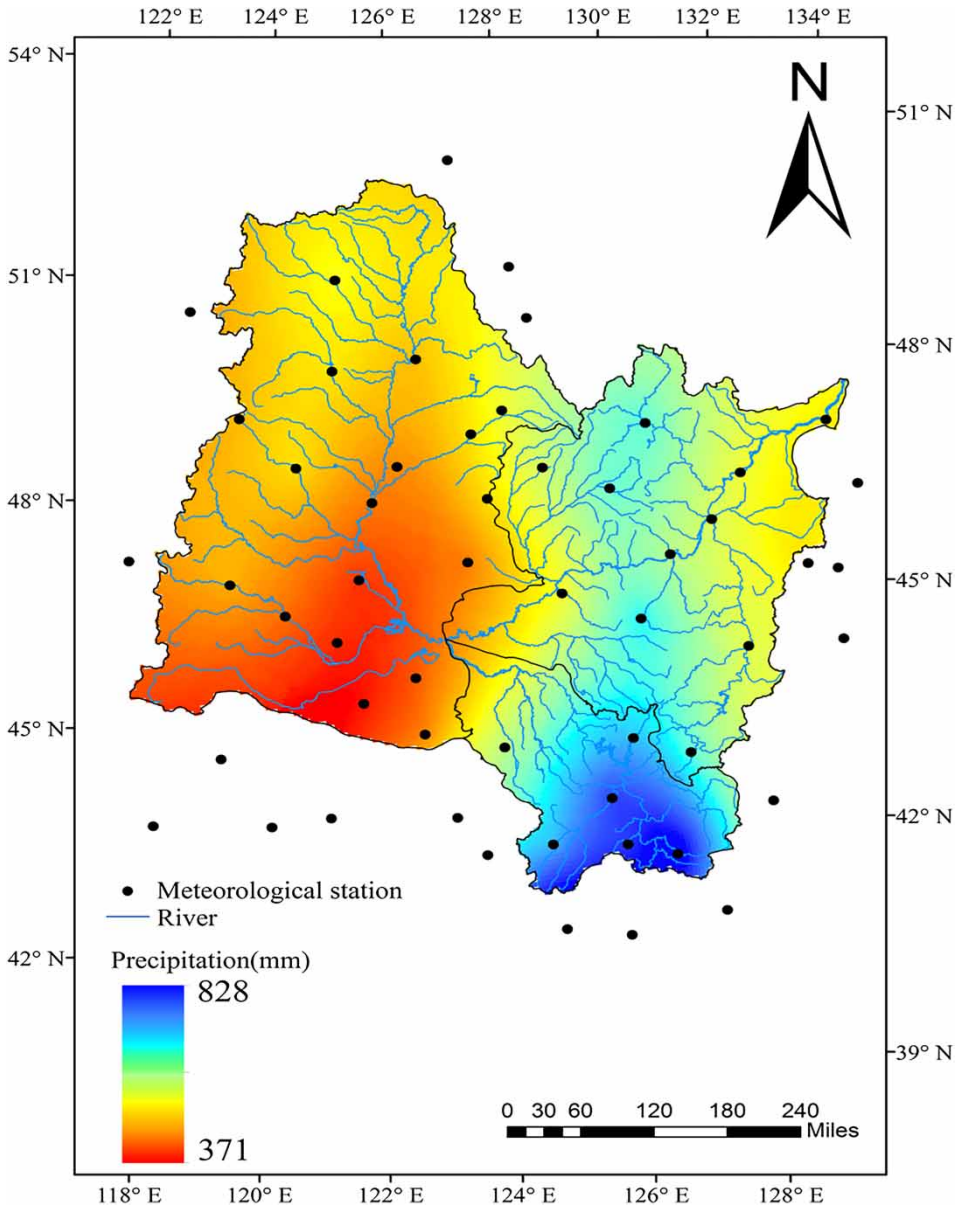

Figure 2 | Spatial distribution of annual precipitation in the SRB.

of precipitation changes in the SRB and to provide an important reference for the sustainable development of regional water resources and water resource management and planning for the study of precipitation variation in the SRB, we studied not only the annual precipitation but also the precipitation in different seasons. In this chapter, when analysing seasonal precipitation, we divide the four seasons into spring (March–May), summer (June–August), autumn (September–November) and winter (December–February).

Spatial and temporal distributions of annual precipitation

In Figure 2, the spatial distribution of the average annual precipitation over the SRB from 1960 to 2013 is illustrated with kriging interpolation in ArcGIS. Figure 2 indicates that the spatial distribution of precipitation is quite varied in the SRB. High-precipitation values are concentrated at approximately 127–129°E in the eastern part of the SRB. The precipitation shows a decreasing trend from east to

west. Dongjiang Station in the USRB has the largest annual average rainfall (827.88 mm) in the entire SRB, which is 1.91 times the minimum annual mean precipitation (433.79 mm) at Anda Station in the LSRB and 2.18 times the minimum annual mean precipitation (379.55 mm) at Tongyu Station in the NRB. The spatial distribution of annual precipitation directly leads to precipitation differences in each sub-basin. The average annual precipitation is the largest in the LSRB, the second largest in the USRB and the smallest in the NRB.

To further analyse the trends in annual precipitation changes, the simple linear regression test, MK trend analysis and Sen's slope method were used to calculate the time series of average annual precipitation at each station from 1960 to 2013. Simple linear regression tests can well reflect the quantitative relationships between research elements. Positive or negative values of the statistic S represent increasing or decreasing precipitation trends. Sen's slope method is a good way to describe the magnitude of the trend. Positive or negative β values calculated with Sen's slope method represent an annual increase or decrease in precipitation. The Z value calculated with the MK trend analysis method can test for the significance of the change. When Z is greater than 1.96 or less than 1.96, the trend is significant at the 95% confidence level. The results of the calculations are shown in Table 2.

As shown in Table 2, among the 35 stations, statistic S was positive for 19 stations and negative for 16 stations. The β values are positive at 20 stations and negative at 15 stations. These data indicate an increase in precipitation at most stations in the river basin, which is consistent with a report published by the IPCC, noting that precipitation has increased between 30 and 85°N throughout the 20th century. The magnitude of the β value indicates the size of the trend. According to the results (Table 2) of the MK trend analysis and Sen's slope method, the annual precipitation increase was largest in Jiagedaqi at 1.58 mm/a. The largest reduction in annual precipitation was found in Shangzhi at −1.71 mm/a. The range of the Z values calculated via the MK trend analysis is −1.55 to 1.27, so the average annual precipitation change is not significant. The simple linear regression results are consistent with the results of Sen's slope method (Figure 2 and Table 2), except that the signs of the values calculated with the two methods are opposite for Meihekou. However, the difference between S and β at Meihekou was relatively small and thus might not have a major impact on the trend of the average annual precipitation series (She *et al.* 2016).

To better analyse the variation in precipitation in the SRB, MK analysis was used to analyse the average annual precipitation in each sub-basin. As shown in Figure 3, the SRB shows an initial decreasing trend, followed by an

Table 2 | Sen's slope β and statistic S of the mean annual precipitation at each station during 1960–2013

Area	Name	Slope β (mm/a)	Statistic S	Area	Name	Slope β (mm/a)	Statistic S
LSRB	Dunhua	−0.36	−0.79	NRB	Anda	0.90	0.80
	Hailun	0.13	0.12		Mingshui	0.98	0.80
	Tieli	−1.40	−1.05		Jiagedaqi	1.58	2.08
	Yichun	−0.04	−0.33		Nenjiang	−0.10	−0.14
	Harbin	0.35	0.61		Xiaoergou	0.66	0.60
	Tonghe	−1.06	−1.54		Beian	0.14	0.35
	Yilan	0.12	0.02		Keshan	1.00	1.06
	Jiamusi	0.36	0.83		Boketu	0.08	0.38
	Fujin	−0.38	−0.44		Zhalantun	0.61	0.66
	Shangzhi	−1.71	−1.49		Fuyu	−0.002	−0.25
	Mudanjiang	0.49	0.58		Qiqihar	1.12	1.01
USRB	Jingyu	0.81	0.38		Tailai	0.40	0.44
	Changchun	0.47	0.07		Suolun	−0.46	−0.48
	Jiaohe	−0.37	−0.70		Wulanhaote	−0.06	−0.09
	Donggang	0.42	0.26		Baicheng	−1.23	−1.53
	Huadian	1.06	0.67		Qianan	−0.46	−1.00
	Meihekou	0.12	−0.12		Tongyu	−1.68	−1.41
					Changling	−1.51	−1.53

Note: '*' indicates that the trend shows a significant change ($Z \geq 1.96$ or $Z \leq -1.96$).

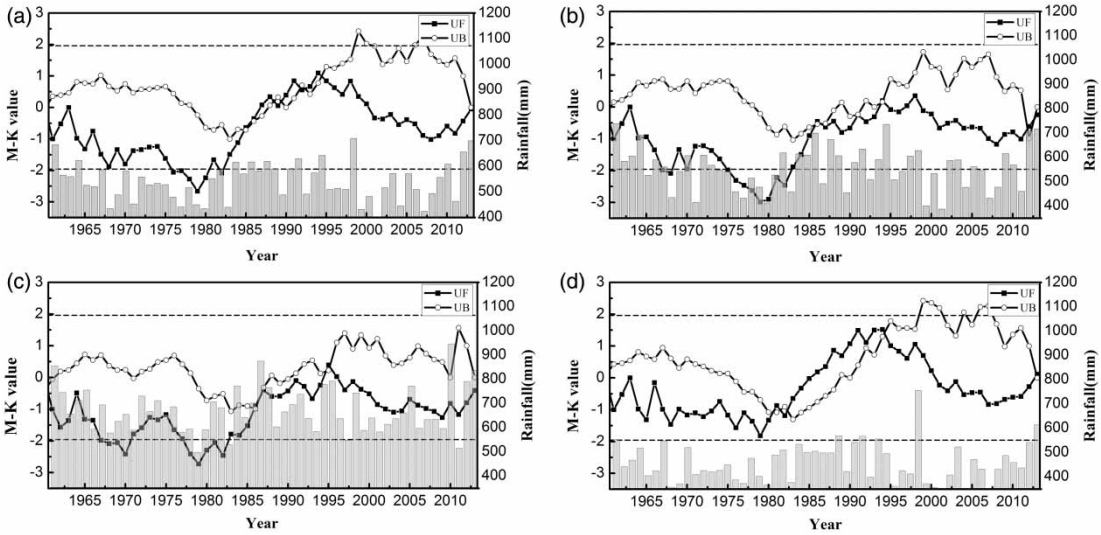

Figure 3 | The MK average annual precipitation trends in (a) the SRB, (b) the LSRB, (c) the USRB, and (d) the NRB.

increase and subsequent decrease. This abrupt shift occurred in 1986 and again in 1994. The first Songhua River, the second Songhua River and the NRB all show a tendency for the average annual precipitation trend to initially decrease, then increase and finally decrease again. The first Songhua River shows a decreasing trend from 1960 to 1986, with a significant decrease from 1975 to 1983, an abrupt change in 1987 and then an upward trend in 1994, which is not significant. Finally, the river slightly decreased again after 1994. The second SRB shows a decreasing trend from 1960 to 1986, decreasing significantly from 1977 to 1983, and a nonsignificant increasing trend from 1986 to 1995. Finally, the river decreased slightly after 1995. The NRB shows a slight decreasing trend from 1960 to 1982, followed by an increasing trend until 1994 and a subsequent decreasing trend after 1994, which does not exceed the 95% confidence level; therefore, the change is not significant.

Spatial and temporal distributions of seasonal precipitation

The spatial distribution of seasonal average precipitation in the SRB from 1960 to 2013 as visualized by the kriging interpolation method in ArcGIS is shown in Figure 4. The spatial distributions of seasonal precipitation in the basin were similar. The regions with high precipitation are located in the southeast of the SRB, the regions with low precipitation are located in the east and northwest of the basin, and the areas with the lowest precipitation are located in the southwest and middle of the basin. The seasonal average precipitation at Donggang Station in the southeast of the basin is the maximum for all seasons. In each season, the precipitation in the USRB is the largest, followed by that in the LSRB, whereas the NRB has the lowest amount of precipitation. The results are consistent with the average annual precipitation in each sub-basin.

To further analyse the trends in the seasonal precipitation changes, the MK trend analysis method, the simple linear regression method and Sen's slope method were used to calculate the seasonal precipitation at each station. The Z value calculated by the MK trend analysis method was used to determine the significance of the change. Sen's slope estimator β and the S and Z statistics calculated for the quarterly average precipitation at each site are shown in Table 3.

It is clear from Table 3 that the results obtained for statistic S and slope value β are basically the same, with few results showing differences and no results showing significant differences. The differences may not have much effect on the trend of the average seasonal precipitation series. In the spring, precipitation in most areas of the SRB shows an increasing trend (29/35). The largest increase is found at Donggang Station in the USRB, with an increase of 0.63 mm/year. Except for the significant increases in precipitation in Wulanhaote ($Z = 2.12$) and Changchun

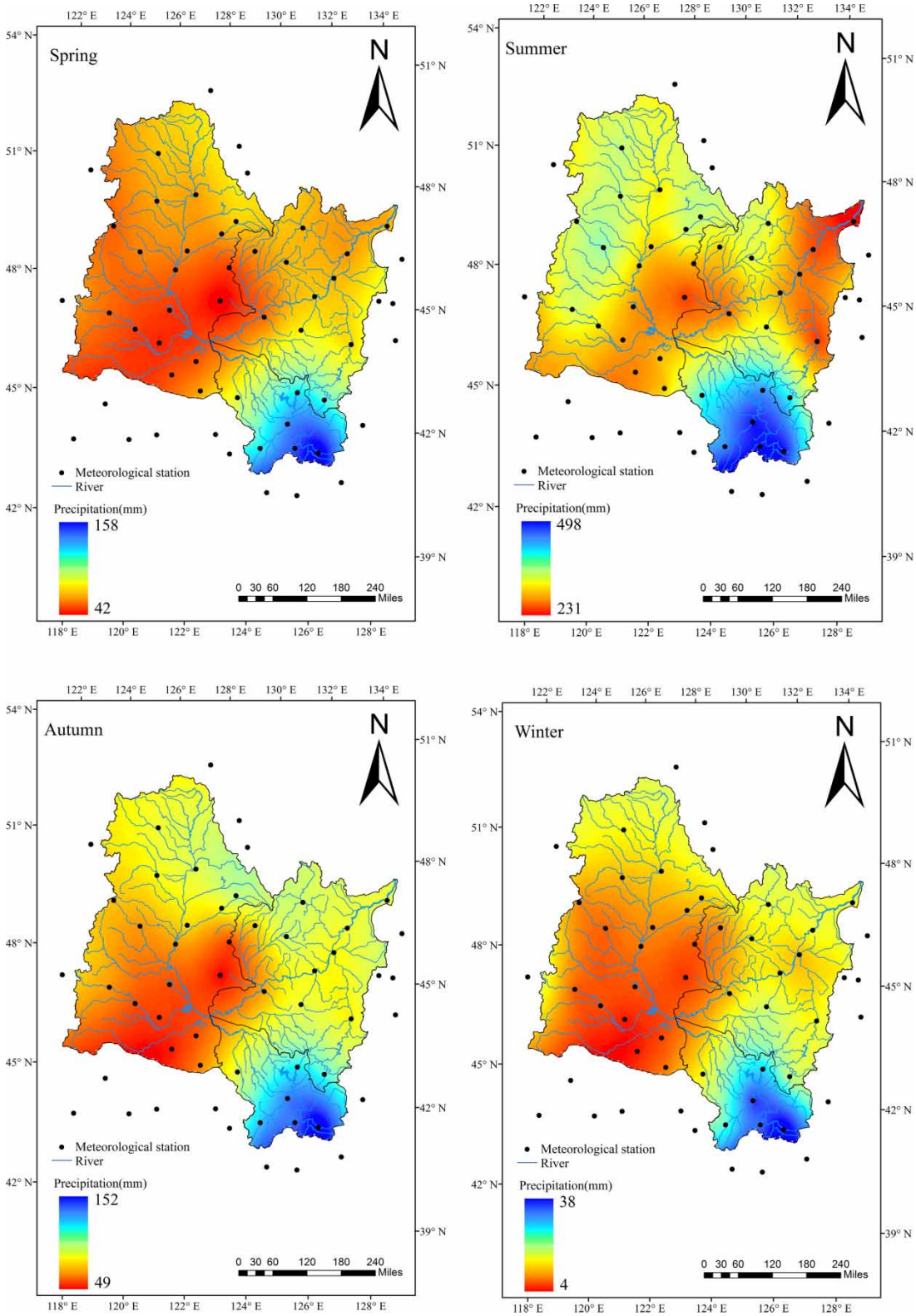

Figure 4 | Spatial distributions of seasonal precipitation in the SRB (spring – MAM, summer – JJA, autumn – SON, winter – DJF).

Table 3 | Sen's slope β and statistic S of the mean seasonal precipitation at each station during 1960–2013

		Spring		Summer		Autumn		Winter	
Area	**Name**	**Slope β (mm/a)**	**Statistic S**	**Slope β (mm/a)**	**Statistic S**	**Slope β (mm/a)**	**Statistic S**	**Slope β (mm/a)**	**Statistic S**
LSRB	Hailun	−0.06	−0.06	−0.13	−0.21	−0.2	−0.13	0.11*	0.12
	Tiele	0.14	0.12	−1.3	−1.40	−0.09	−0.04	0.12*	0.12
	Yichun	0.09	0.08	−0.64	−0.85	−0.03	0.09	0.16*	0.17
	Harbin	0.23	0.28	−0.28	−0.16	−0.10	−0.15	0.05	0.06
	Tonghe	−0.24	−0.24	−0.95	−0.96	−0.24	−0.33	0.02	0.02
	Yilan	−0.01	−0.07	−0.09	−0.09	−0.23	−0.12	0.11*	0.14
	Jiamusi	0.20	0.31	−0.77	0.30	0.08	0.20	0.14*	0.17
	Fujin	0.17	0.27	−1.03	−1.01	−0.04	−0.04	0.11*	0.15
	Shangzhi	−0.03	−0.06	−1.39	−1.79	−0.26	−0.25	0.12*	0.15
	Mudanjiang	0.29	0.29	−0.3	−0.3	−0.23	−0.17	0.04*	0.15
	Dunhua	0.44	0.45	−0.91	−1.04	−0.02	0.06	0.08*	0.17
USRB	Changchun	0.60*	0.67	−0.13	−0.09	−0.30	−0.40	0.15*	0.27
	Jiaohe	0.23	0.31	−0.64	−0.52	−0.39	−0.35	0.08	0.14
	Huadian	0.31	0.31	0.75	0.99	−0.20	−0.29	0.16	0.32
	Meihekou	0.15	0.15	−0.07	−0.07	−0.03	−0.10	0.10	0.16
	Jingyu	0.30	0.30	0.76	1.13	−0.54	−0.60	0.07	0.19
	Donggang	0.63	0.63	−0.59	−0.32	−0.01	−0.02	0.13*	0.21
NRB	Jiagedaqi	0.49	0.44	1.70	0.90	0.46	0.43	0.13*	0.16
	Nenjiang	0.16	0.22	−0.38	−0.31	−0.23	−0.16	0.05	0.10
	Xiaoergou	0.40	0.40	0.53	0.37	−0.22	−0.19	0.09*	0.11
	Beian	0.13	0.30	0.26	0.30	−0.56	−0.55	0.09*	0.14
	Keshan	0.19	0.25	0.59	0.89	−0.23	−0.23	0.12*	0.04
	Boketu	0.30	0.26	−0.18	−0.30	0.06	0.06	0.94*	1.08
	Zhalantun	0.42	0.56	−0.33	−0.30	−0.01	−0.01	0.10*	0.17
	Fuyu	−0.04	−0.04	−0.13	−0.35	−0.49	−0.49	0.13*	0.14
	Qiqihar	0.28	0.43	0.42	0.61	−0.26	−0.26	0.16*	0.17
	Tailai	0.44	0.61	−0.26	−0.06	−0.34	−0.34	0.14*	0.14
	Suolun	0.23	0.25	−0.65	−0.48	−0.36	−0.36	0.09*	0.10
	Wulanhaote	0.60*	0.67	−0.61	−0.57	−0.27	−0.27	0.06*	0.10
	Baicheng	0.38	0.49	−1.89*	−1.69	−0.15	−0.15	0.03	0.06
	Qianan	0.04	0.18	−0.17	−0.62	−0.02	−0.02	0.01	0.03
	Tongyu	0.21	0.46	−2.06*	−1.98	−0.12	−0.22	0.57	0.65
	Anda	0.13	0.18	0.48	0.38	−0.4	−0.34	0.03	0.03
	Mingshui	−0.11	−0.10	0.29	0.43	−0.15	−0.11	0.01	0.01
	Changling	0.10	0.27	−1.67*	−1.77	−0.23	−0.05	0.04	0.11
Statistic S	Increase	29	29	9	10	3	5	35	35
	Decrease	6	6	26	25	32	30	0	0

Note: '*' indicates that the trend shows a significant change ($Z \geq 1.96$ or $Z \leq -1.96$).

($Z = 1.98$), the Z values calculated for spring using the MK method range from −0.75 to 1.7, and none of them exceeds the 95% level of significance, indicating that the trends for spring precipitation in the basin are not significant. In the summer, precipitation in most parts of the drainage area shows a decreasing trend (26/35). The largest reduction in precipitation is at the NRB's Tongyu Station, with a decrease of 2.06 mm/year. Except for the significant decreases in precipitation in Changling ($Z = -2.28$), Baicheng ($Z = -2.31$) and Tongyu ($Z = -2.39$), the Z values calculated for summer using the MK method range from −1.19 to 1.21, and none of them exceeds the 95% significance level, indicating that the trends of summer precipitation in the basin are not significant. In the autumn, precipitation in most parts of the basin shows a decreasing trend (32/35). The Z values range from −1.83 to 0.68, and none of them exceeds the 95% significance level, indicating that the trends of precipitation change in

the autumn are not significant. In the winter, precipitation in the whole basin shows an increasing trend. The Z values range from 0.27 to 3.06, and the precipitation increases in most areas exceed the 95% significance level, indicating that precipitation increases significantly in most areas during the winter. Generally, the spring precipitation in most areas does not increase significantly. In the summer and autumn, the precipitation in most areas does not significantly decrease, but in the autumn, the area with decreased precipitation is larger. In the winter, the precipitation in the whole basin shows an increasing trend, and the increase in precipitation is significant in most areas. These results are consistent with Lu's conclusion (Lu *et al.* 2012).

Spatial and temporal variability of dryness/wetness during 1960–2013

Drought is a complicated phenomenon. It affects not only regional water resources but also agricultural production. The SRB is an important food production base in China. Therefore, it is important to study dry/wet changes in the SRB. Therefore, in this study, long-term SPI24 and short-term SPI3 were used to determine the dry and wet changes and frequent drought and flood areas in the SRB. These data provide an important basis for water resource management and planning under the background of global warming in the SRB and the formulation of drought and flood control measures and agricultural production planning.

Long-term spatial and temporal variability of dryness/wetness

To determine the spatial distribution patterns of dry/wet in the SRB and to provide a basis for the management and planning of water resources in the SRB, we applied a rotating PCA to the SPI time series at the 24-month time scale (SPI24) at each station in the SRB to classify the stations with the same dry and wet change characteristics. The satisfactory cumulative variance percentage was set to approximately 70% (Huang *et al.* 2014, 2015; Fu *et al.* 2018a, 2018b; Guo *et al.* 2018). As shown in Table 4, the cumulative variance for five principal components was 72.63%. Therefore, it was reasonable to choose five principal components. Relevant rotational loads are displayed

Table 4 | Explained variance of the first five principal components

Component	Variance	Cumulative explained variance
1	18.29	18.29
2	15.98	34.27
3	14.34	48.61
4	13.47	62.08
5	10.55	72.63

in space by the kriging method in ArcGIS, as shown in Figure 5. According to Li & Wang (2016), the reasonable threshold value is 0.6 for rotated loadings, which can reflect the general evolution of dry and wet events in different sub-regions.

As shown in Figure 5(a)–5(e), the five sub-regions considered to analyse the variational characteristics of dry/wet events in the SRB include the south-western area of the SRB, the central SRB, the eastern area of the SRB, the south-eastern area of the SRB and the north-western area of the SRB. Figure 5(f)–5(j) shows the sub-regional changes in the dryness/wetness conditions. The wet trends are mainly concentrated in the central, south-eastern and north-western parts of the SRB (Figure 5(b), 5(d) and 5(e)), and the dry trends are concentrated in the south-western and eastern parts of the SRB (Figure 5(a) and 5(f)). The patterns of wet and dry changes may be related to the complicated topography of the SRB and the spatial structure of the large-scale atmospheric circulation patterns. The SRB is surrounded by mountains on three sides. A wide range of southeast, southwest or southern winds prevails throughout the year. The barrier effect of the Changbai Mountains and the Greater Khingan Mountains on these prevailing winds results in rich precipitation in the mountainous areas and relatively little precipitation on the plains (Shu *et al.* 2007). Thus, the dry/wet patterns shown in Figure 5 are formed. In summary, the PCA has well divided the SRB into five different sub-regions with different patterns of dry/wet changes. Therefore, to conduct reasonable and effective water resource management under the background of climate change, these sub-regions should be considered separately.

Further investigations were carried out according to the categories shown in Table 1 to determine the dry/wet variations in the SRB. The numbers of dry/wet months in different categories at each station were counted and

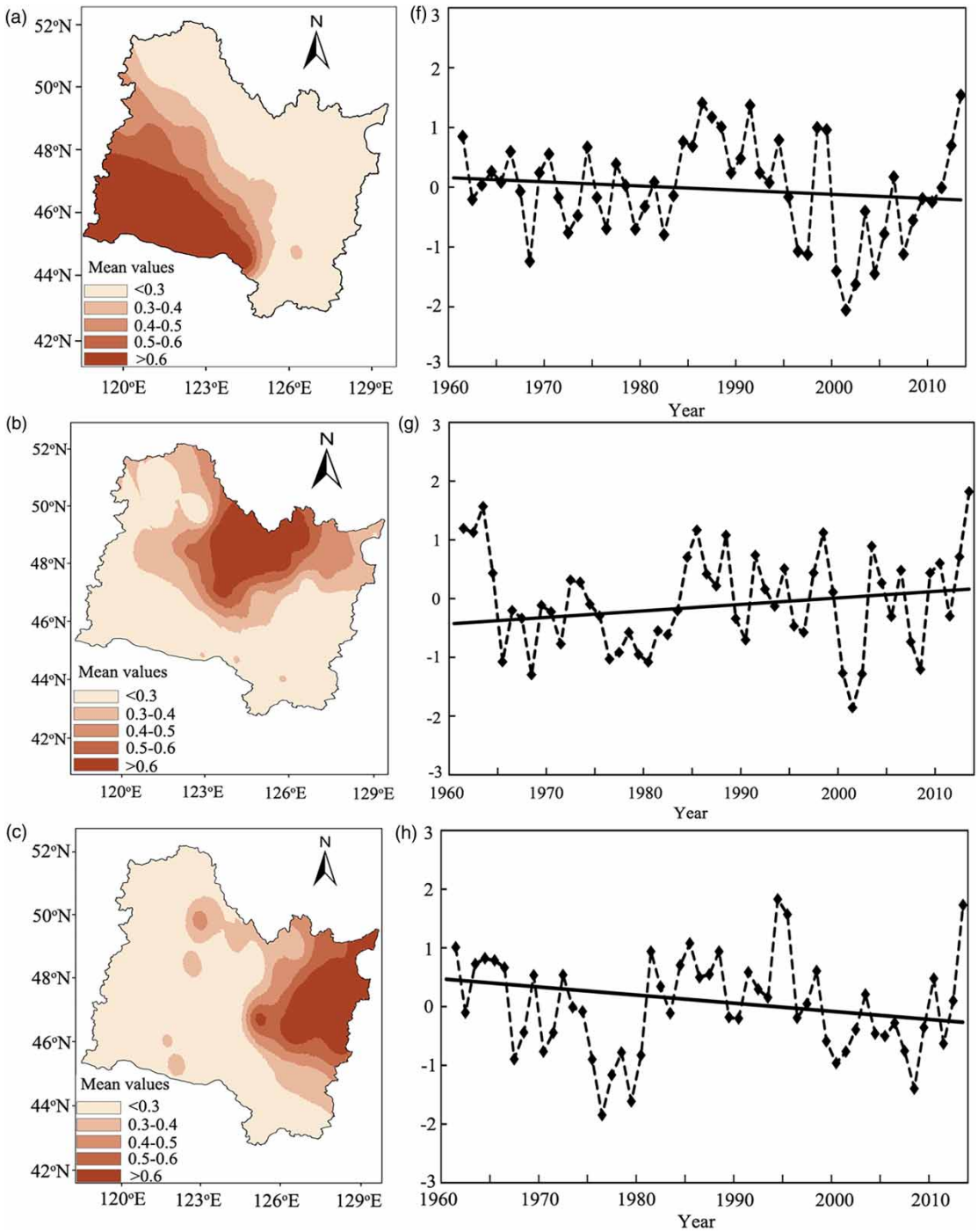

Figure 5 | The first five rotated loadings (a–e) and corresponding SPI24 series (f–j) from 1960 to 2013. (*Continued*).

analysed by the MK method. The trends were calculated as follows: (1) The numbers of dry/wet months in the SPI24 time series within each year were counted. (2) The time series of the number of months in each category in each year was constructed, and the trend Z values for the time series were calculated using the MK trend method. With ArcGIS, different symbols were used to indicate increasing and decreasing trends. Figure 6(a)–6(f) shows the spatial

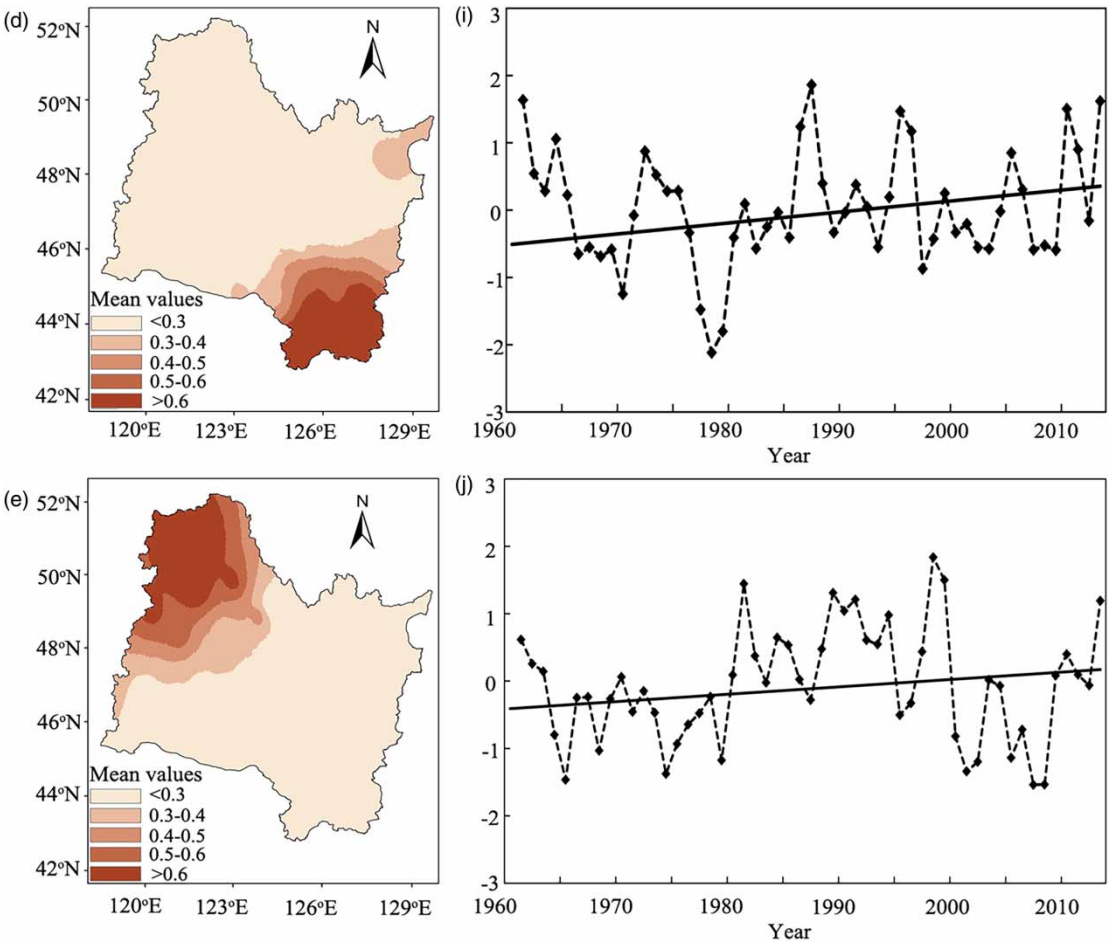

Figure 5 | Continued.

distribution patterns of the numbers of dry/wet months in different categories during the study period.

In general, the dry/wet change trends in the SRB are varied. The numbers of extremely, severely and moderately dry months show increasing trends in most of the southwestern SRB. The numbers of extremely and severely dry months show increasing trends in most of the eastern SRB. Meanwhile, the numbers of severely and moderately wet months show an increase in most areas from the northeast to the southwest of the SRB. The numbers of extremely wet months show increasing trends in some central parts of the SRB. However, these changes are not significant. The variation trends of the dry/wet months agree well with the spatial distributions of the dry/wet patterns in the SRB (Figure 5). The trend towards wetter conditions has helped mitigate the risk of drought. These data show that there is an increasing trend in the number of dry months in the east and southwest, indicating that the meteorological drought risk in these regions may be increasing. Meanwhile, the number of wet months is increasing from the southeast to the northwest, indicating that the risk of flooding in these regions is likely to increase. Previous studies have also reported similar findings. The frequency of drought in the east and southwest of the SRB is relatively high, whereas the flood frequency from southeast to northwest is relatively high (Han *et al.* 2014).

Short-term spatial and temporal variability of dryness/wetness

The short-term time scale SPI3 was used to analyse seasonal dry and wet changes in the SRB. The Z value of the SPI3 time series for each station in each season was calculated

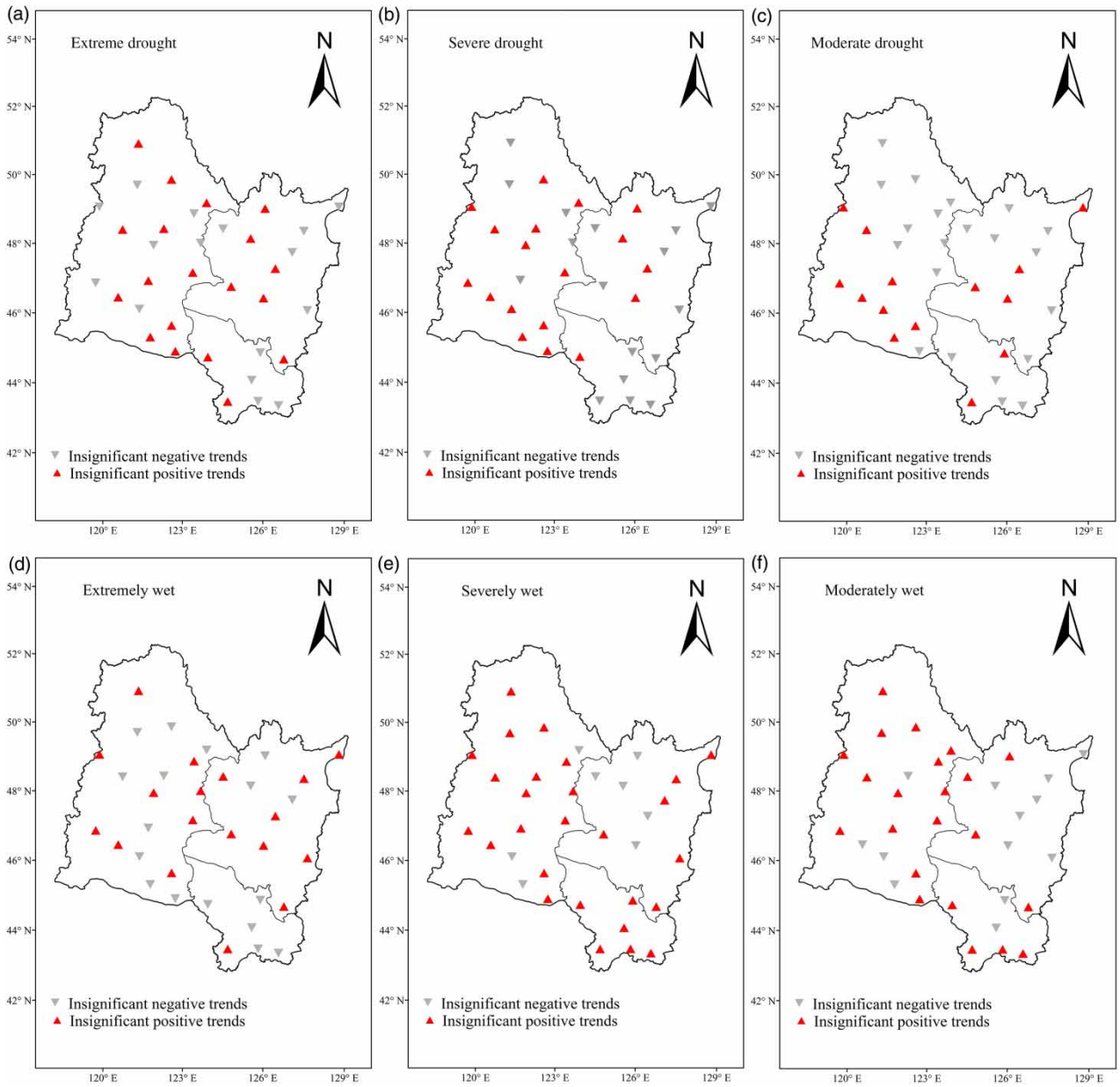

Figure 6 | Spatial distributions of the trends in the numbers of wet and dry months for different categories.

using MK trend analysis, and the results are shown in Figure 7. Figure 7(a)–7(d) represents the variation trends in the SPI3 time series for each station in the spring, summer, autumn and winter.

The changes in SPI3 in the spring, autumn and winter show good consistency (Figure 7). In the spring, almost all the stations in the basin show increasing trends, and a few of them show significant increasing trends. In the summer, most areas show a decreasing trend. Some stations in the southwest of the SRB show significantly decreasing trends, while some areas in the middle of the SRB show slightly increasing trends. These different trends may be due to changes in the land use/cover patterns of agriculture to forest (grass), which increases precipitation and slows the trend of precipitation reduction (Li *et al.* 2017). In the autumn, except for two stations in the north-western part of the SRB, no significant increasing precipitation trends were found. Almost all the stations in the basin show decreasing

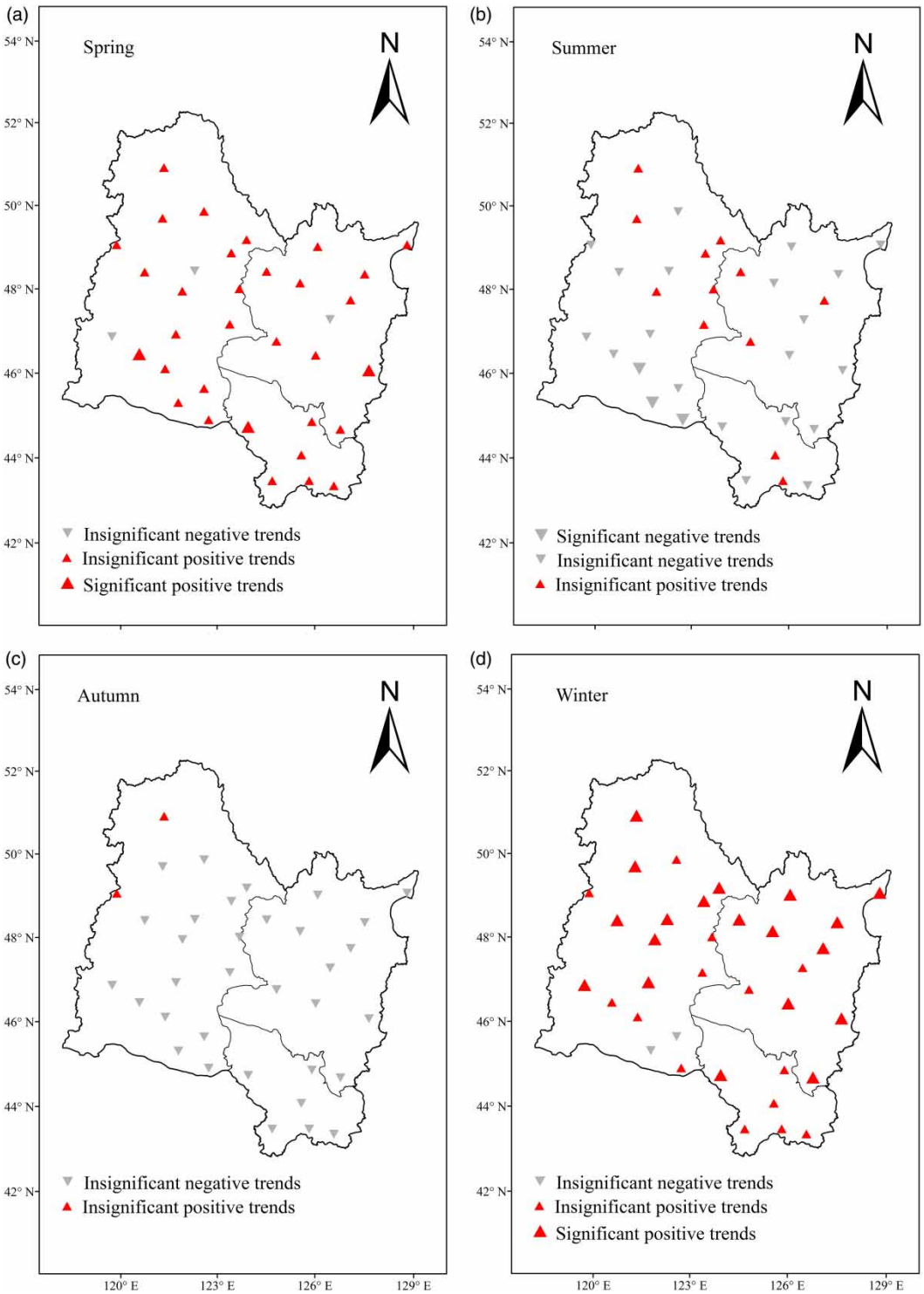

Figure 7 | Spatial distributions of the SPI3 trends at each station ((a) spring – MAM; (b) summer – JJA; (c) autumn – SON; (d) winter – DJF)).

trends, but the trends are not significant. In the winter, except for two stations in the southwest, there are no significant trends of decreasing precipitation. The rest of the stations show increasing trends, and most of these trends are

significant. Therefore, from the perspective of the short-term time scale, SPI3, the seasonal dry and wet changes in the SRB show strong seasonal characteristics. In general, there is no significant wetting trend in the spring. There is also no significant drought trend in the summer or autumn, although drought is more widespread in the autumn. In the winter, there is a significant wetting trend. The seasonal dry/wet changes are consistent with the results of Feng *et al.* (2016).

To further understand the dry/wet changes in the SRB to provide guidance for agricultural development, we conducted an analysis based on the SPI categories as shown in Table 1. The numbers of dry/wet months in different categories at each station were counted and analysed by the MK method. The trends were calculated as follows: (1) The numbers of dry/wet months in the SPI3 time series within each season were counted. (2) The time series of the number of months in each category in each season was constructed, and the trend Z values for the time series were calculated using the MK trend method. Table 3 shows the trends of the numbers of wet and dry months in different categories in each sub-region.

As shown in Table 5, the numbers of dry months in all three categories showed increasing trends in spring and winter, and the numbers of wet months in all three categories showed decreasing trends. However, they do not exceed 95% significance, indicating that these trends are not significant. The trends of the numbers of wet/dry months in each category in the summer and autumn are opposite to those in the spring and winter. However, in the NRB, the numbers of severely and moderately dry months show significant increasing trends. The numbers of extremely dry months also show increasing trends, but these trends are not significant. The changes in the numbers of dry/wet months in each category are consistent with the description of seasonal drought changes in the SRB given by Feng *et al.* (2016). The significant increases in the numbers of moderately and severely dry months in the NRB in autumn are consistent with the data previously published by Feng *et al.* (2016) on the division of areas with a high drought risk in the SRB (Li *et al.* 2017).

Table 5 | Trends of the numbers of wet and dry months in different categories in each sub-region

Area	Category	Spring	Summer	Autumn	Winter
LSRB	Extremely dry	0.61	0.40	0.45	−0.60
	Moderately dry	−0.26	0.93	1.22	−0.05
	Moderately dry	−0.31	0.73	1.09	−0.75
	Moderately wet	0.98	0.65	−0.32	0.22
	Severely wet	0.90	−0.09	−0.76	0.93
	Extremely wet	0.62	−0.53	−0.66	0.70
	Extremely dry	−0.90	0.51	0.57	−0.46
	Moderately dry	−0.07	0.69	0.42	−0.58
USRB	Moderately dry	−1.11	1.61	0.94	−0.71
	Moderately wet	0.66	−0.34	−1.16	0.04
	Severely wet	1.32	−0.46	−0.78	0.58
	Extremely wet	0.70	−0.27	−0.51	0.46
	Extremely dry	−0.52	0.52	1.08	−0.60
	Moderately dry	−0.72	0.82	1.97*	−0.38
NRB	Moderately dry	−1.50	0.54	2.01*	−0.10
	Moderately wet	1.15	0.72	−0.38	0.45
	Severely wet	0.78	−0.44	0.30	0.34
	Extremely wet	0.74	−0.34	−0.26	1.48

Note: '*' indicates that the trend shows a significant change ($Z \geq 1.96$ or $Z \leq -1.96$).

Changes in annual and monthly precipitation in various steps and correlations

The change in annual precipitation is mainly caused by the change in precipitation over 1 month or a defined period. Therefore, studies of changes in precipitation over these periods are important. This paper quantifies the contribution of monthly precipitation to annual precipitation in the SRB. The stepwise changes in annual mean precipitation (Figure 8) and monthly precipitation (Figure 9) in the SRB were studied. Studies of the change in monthly precipitation provide a deeper understanding of the characteristics of precipitation in the SRB and also deepen our understanding of changes in the precipitation pattern of the SRB. This study provides an important reference for the sustainable development of regional water resources, water resource management and planning, and drought and flood prevention.

According to the MK trend analysis of the SRB and the tributaries shown in Figure 4, the average annual precipitation period in the SRB can be divided into four sub-periods ($P_{\text{Period1}} = 1960–1986$, $P_{\text{Period2}} = 1987–1994$, $P_{\text{Period3}} = 1995–2013$ and $P_{\text{Period4}} = 1960–2013$). From Figure 8, we see that from Period 1 to Period 2 in the LSRB, USRB, NRB and SRB, precipitation increased by 86.96, 73.6, 95.7 and 82.62 mm, respectively. From Period 2 to Period 3 in the LSRB, USRB, NRB and SRB, precipitation decreased by 93.37, 51.46, 104.5 and 88.57 mm, respectively. The change in precipitation during Period 2 is the greatest among the three sub-periods.

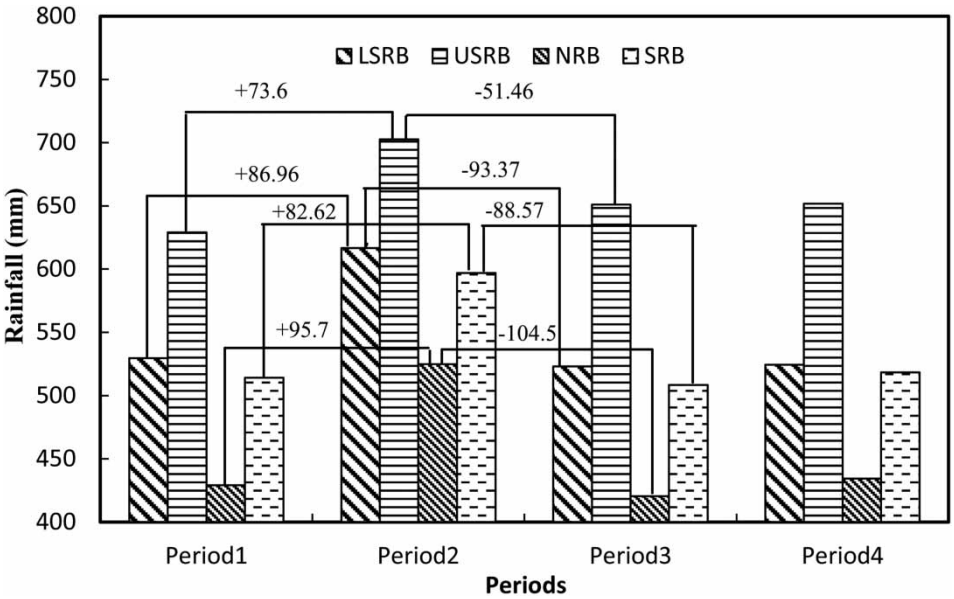

Figure 8 | The mean annual rainfall in P_{Period1} (1960–1986), P_{Period2} (1987–1994), P_{Period3} (1995–2013) and P_{Period4} (1960–2013) in the LSRB, USRB, NRB and SRB.

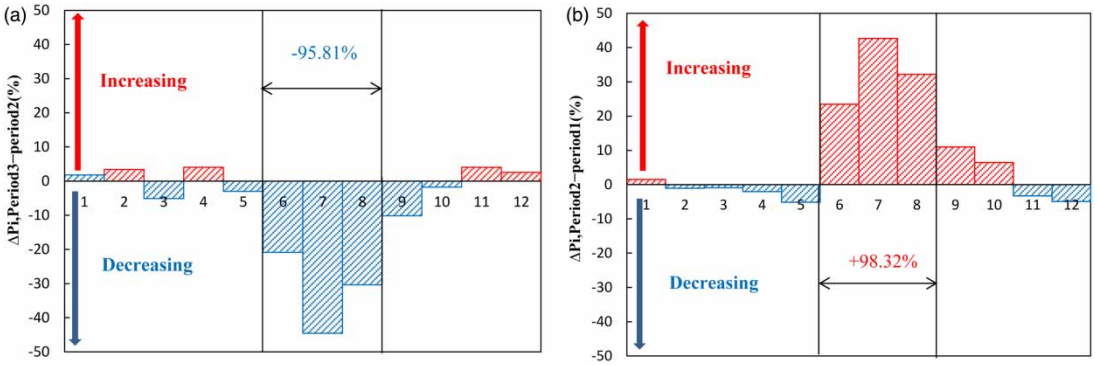

Figure 9 | Monthly average precipitation changes during each sub-period. (a) Period 1 to Period 2; (b) Period 2 to Period 3.

There is no obvious change in the overall precipitation throughout the time series. However, between different sub-periods, there are stepwise changes in precipitation.

To study the contribution of the monthly precipitation to the average annual precipitation, the monthly precipitation contribution to the annual precipitation is defined as follows:

$$\Delta P_{i,\text{Period2}-\text{Period1}} = \frac{P_{i,\text{Period2}} - P_{i,\text{Period1}}}{P_{\text{Period2}} - P_{\text{Period1}}} \times 100\% \quad (i = 1, 2, \ldots, 12) \tag{15}$$

$$\Delta P_{i,\text{Period3}-\text{Period2}} = \frac{P_{i,\text{Period3}} - P_{i,\text{Period2}}}{P_{\text{Period3}} - P_{\text{Period2}}} \times 100\% \quad (i = 1, 2, \ldots, 12) \tag{16}$$

where P_{Period1}, P_{Period2} and P_{Period3} represent the average annual precipitation for each time period and $P_{i,\text{Period1}}$, $P_{i,\text{Period2}}$, and $P_{i,\text{Period3}}$ represent the average precipitation in the ith month of each time period. Based on Figure 8, $P_{\text{Period2}} - P_{\text{Period1}}$ and $P_{\text{Period3}} - P_{\text{Period2}}$ are 82.62 and −88.57 mm, respectively. The positive and negative values of $\Delta P_{i,\text{Period2}-\text{Period1}}$ and $\Delta P_{i,\text{Period3}-\text{Period2}}$ represent the increasing or decreasing trends in average precipitation during the ith month in each time period, respectively. The changes in precipitation in the ith month during each sub-period are shown in Figure 7.

The values of $\Delta P_{i,\text{Period2}-\text{Period1}}$ in Figure 9(a) indicate that the contribution of the monthly precipitation to the

annual precipitation increases during June, July, August, September and October, whereas the precipitation contribution during other months decreases; the increase is much larger than the decrease. The $\Delta P_{i,\text{Period2}-\text{Period1}}$ values over 6–8 months are greater than 20%, which means that the increase in precipitation mainly occurred during these months from Period 1 (1960–1986) to Period 2 (1987–1994). The monthly increment is at least 20% of the total increase. The precipitation increases between June and August account for 98% of the total precipitation increase, which indicates that the change in precipitation from Period 1 to Period 2 occurred mainly between June and August. Similar conclusions can be drawn from Figure 9(b). The decrease in the annual mean precipitation from Period 2 to Period 3 is mainly concentrated between June and August.

According to the results shown in Figure 9, a year can be divided into two parts in this study. June–August is representative of the rainy season (RS), and the remaining months of the year represent the non-rainy season (Non-RS). The calculated precipitation during the RS accounts for 76% of the average annual precipitation. Therefore, the RS precipitation in the SRB may play an important role in the annual changes. The following will further show the relationship between the RS precipitation and the average annual precipitation. To better analyse the effects of monthly precipitation on annual precipitation, the relationships between precipitation during the RS, precipitation during the non-monsoon season and annual precipitation were analysed and shown in Figure 10.

Figure 10(a) shows the variation pattern in the RS precipitation, which is similar to that of the average precipitation shown in Figure 8. The precipitation was 323.1 mm in Period 1 and increased in Period 2 to 403.42 mm; then, it decreased in Period 3 to 315.33 mm. As shown in Figure 10(b), the patterns of change are quite similar

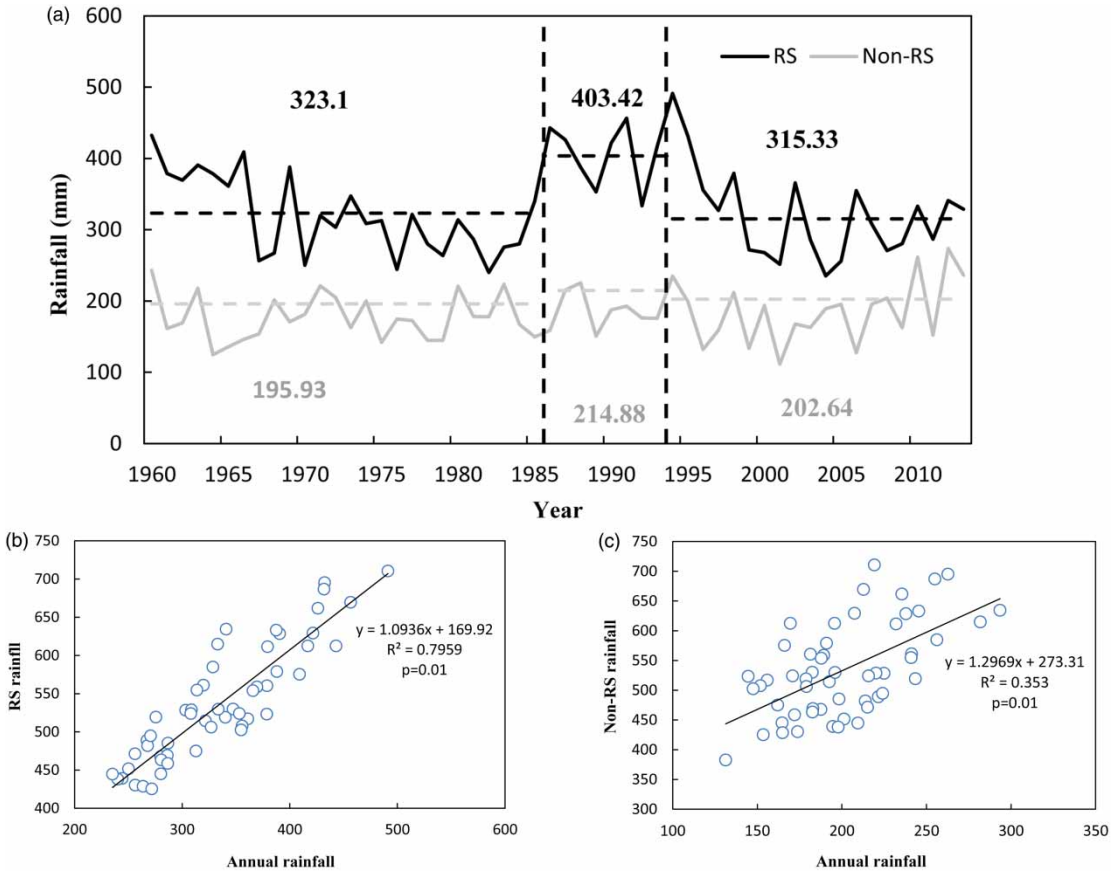

Figure 10 | (a) Variation in precipitation in the RS and Non-RS. (b) Relationship between RS precipitation and average annual precipitation. (c) Relationship between Non-RS precipitation and average annual precipitation.

between the RS rainfall and the annual rainfall ($R2 = 0.796$, $p = 0.01$). However, the changes in precipitation during the Non-RS in the three sub-periods are not obvious. The precipitation was 195.93 mm in Period 1 and increased in Period 2 to 214.88 mm; then, it decreased in Period 3 to 202.64 mm. The variation pattern of the annual rainfall is very different from that of the annual precipitation. The correlation between the Non-RS precipitation and the annual precipitation is relatively low ($R2 = 0.353$, $p = 0.01$), as shown in Figure 10(c). Therefore, the annual precipitation in the SRB is largely due to the change in precipitation during the RS.

Link between the atmospheric circulation pattern and regional precipitation

The causes of precipitation change in eastern China have been investigated in many studies in the literature. The subtropical high is an important atmospheric circulation system that connects the tropics with the temperate regions. The subtropical high swings from north to south with changes in the seasons and is one of the key weather and climate systems in East Asia (He & Gong 2002). Changes in the location and intensity of the subtropical high have affected climate change in China. The Asian meridional/zonal circulation is closely related to drought and flooding in Northeast China. The prevailing zonal circulations are dry and rainy, whereas the prevailing meridional circulations are wet and rainy (Miao & Lin 2004). The weakening of the EASM at the end of the 1970s had a significant effect on the precipitation pattern in China (Xu *et al.* 2013). The PDO was the main contributor to the changes in summer precipitation in eastern China in the 1970s (Lu *et al.* 2014a, 2014b).

The above-mentioned atmospheric circulation pattern had an important impact on precipitation changes in eastern China. The SRB is located in Northeast China (and also in eastern China). So, the atmospheric circulation pattern mentioned above may have had an important impact on the precipitation and wet/dry changes in the SRB. Therefore, in order to determine the main atmospheric circulation patterns affecting precipitation and dry/wet changes in the SRB and to provide a reference for studies of the response of climate change in cold regions to global climate change and a scientific basis for drought early warning systems in cold regions, we chose the WPSI, WPSA, AMCI/AZCI, EASM and PDO to determine the relationship between atmospheric circulation patterns and precipitation in the SRB. We used a partial correlation analysis of the RS (the average annual precipitation and average seasonal precipitation) and the long-term and short-term time series of the dry/wet index (SPI3 and SPI24) for the analysis. According to subsection 'Simple linear regression test method' and Figure 7, we can get that RS and summer are the same period. The precipitation in the SRB basin is mainly concentrated in the RS from June to August, and the characteristics of dry/wet changes in the summer are relatively complex. Therefore, the time series constructed by SPI3 in summer was selected for the study of dry/wet changes in the short time series, and the calculation results are shown in Table 6.

The Asian meridional circulation has an important influence on the variation in dry/wet trends and precipitation in Northeast China (Wang *et al.* 2006). Miao & Lin (2004) showed that changes in the Asian zonal circulation greatly influenced the north-eastern region and the middle and lower reaches of the Yangtze River area. Low Asian zonal circulation values are conducive to flooding in these two regions; otherwise, they are prone to drought. It is evident from Table 6 that the AMCI and AZCI have significant correlations with precipitation and dry/wet changes in the SRB and its sub-regions. Moreover, the correlations between the AMCI and AZCI and the summer precipitation and SPI3 indices exceed the significance level of 0.01, indicating that the AMCI and AZCI have a particularly significant impact on RS precipitation and dry/wet changes in the SRB.

The western Pacific subtropical high is a dominant factor in the East Asian climate and affects temperature and precipitation in most of China (Guo *et al.* 2017; Peng *et al.* 2017). The subtropical high over the western Pacific from July to early August brings the rain belt to north-eastern and northern China, which plays a key role in precipitation and drought in China (Zhao *et al.* 2012a, 2012b). The SRB is located in the middle and high latitudes and on the western edge of the western Pacific subtropical high. The climate change in the SRB is sensitive to the strength and location of the subtropical high (Zhong *et al.* 2017). As shown in Table 6, the WPSI and WPSA are significantly correlated with the average precipitation and RS precipitation in the SRB, and have a significant impact on the dry/wet changes

Table 6 | The correlation coefficients between four precipitation indices and six influencing factors in the SRB

	Annual average precipitation				RS average precipitation				SPI24				SPI3			
	SRB	LSRB	USRB	NRB	SRB	LSRB	USRB	NRB	SRB	LSRB	USRB	NRB	SRB	LSRB	USRB	NRB
WPSI	0.41**	0.36*	0.57*	0.13	0.30*	0.25*	0.42**	−0.04	0.28*	0.21	0.55**	0.04	0.16	0.13	0.40**	−0.03
WPSA	−0.36*	−0.26*	−0.5*	−0.1	−0.16	−0.1	−0.33*	−0.9*	−0.18	−0.11	−0.48*	0.04	−0.07	−0.03	−0.32*	0.08
AMCI	−0.35*	−0.33*	−0.31*	−0.26	−0.46**	−0.57**	−0.42**	−0.37**	−0.46**	−0.47**	−0.36*	−0.36*	−0.54**	−0.56**	−0.43**	−0.40**
AZCI	−0.3*	−0.27**	−0.3*	−0.19	−0.08	−0.46**	−0.20*	−0.50**	−0.35*	−0.36*	−0.27*	−0.32*	−0.51**	−0.46**	−0.22*	−0.51**
EASM	0.32*	0.43*	0.35*	0.03	0.24*	0.45**	0.16*	0.27*	0.17	0.37**	0.18	−0.08	0.20	0.44**	0.15	−0.07
PDO	0.18	0.23	0.02	0.19	−0.07	0.14	−0.04	0.09	0.07	0.12	0.01	0.05	0.12	0.20	−0.04	0.11

Note: '*' and '**' denote significant trends at the 5% and 1% significance levels, respectively.

in the USRB. The WPSI is particularly significantly correlated with the wet/dry changes in the USRB.

Han *et al.* (2015) showed that the EASM index was closely related to summer precipitation because the Mongolian low and the activity of the East Asian trough increased with the increase in activity of the Northeast trough. A strong EASM index value is usually accompanied by a strong ascending motion and the accumulation of water vapour flux caused by precipitation. As shown in Table 6, the EASM index has a significant correlation with the average annual precipitation and RS precipitation and also has a significant influence on the dry/wet changes in the LSRB.

In addition, the PDO is not significantly correlated with precipitation or the dry/wet changes in the SRB, which may indicate that the PDO has little impact on precipitation in the SRB.

To further explain the importance of the six atmospheric circulation indexes for precipitation and dry/wet changes in the SRB, the standardized departures of the atmospheric circulation index series for each station were computed by subtracting the respective RS (June–August) mean from the annual rainfall series for each station and then dividing the values by the respective standard deviation, as shown in Figure 11. The 5-year moving average curve of the standard deviations is also shown in Figure 11. The blue line represents a year in which a step change may occur. They are used to help confirm the relationship between the step changes in precipitation and the atmospheric circulation index.

As shown in Figure 11, from Period 1 to Period 2, the variation of the western Pacific subtropical high was similar to that of precipitation in the SRB. The variation was slightly enhanced and reached its maximum around 1994. The numerical fluctuation of the WPSA is smaller than that of the WPSI. However, Table 6 shows that the WPSI is significantly positively correlated with the precipitation index and that the WPSA is significantly negatively correlated. Therefore, the western Pacific subtropical high is an important factor affecting precipitation in the SRB.

From Period 1 to Period 2, the variation characteristics of the AMCI and AZCI have similar step variation characteristics for precipitation in the SRB, but the change trend is the opposite. In Period 2, the AMCI and AZCI show a decreasing trend. Low Asian zonal circulation values are

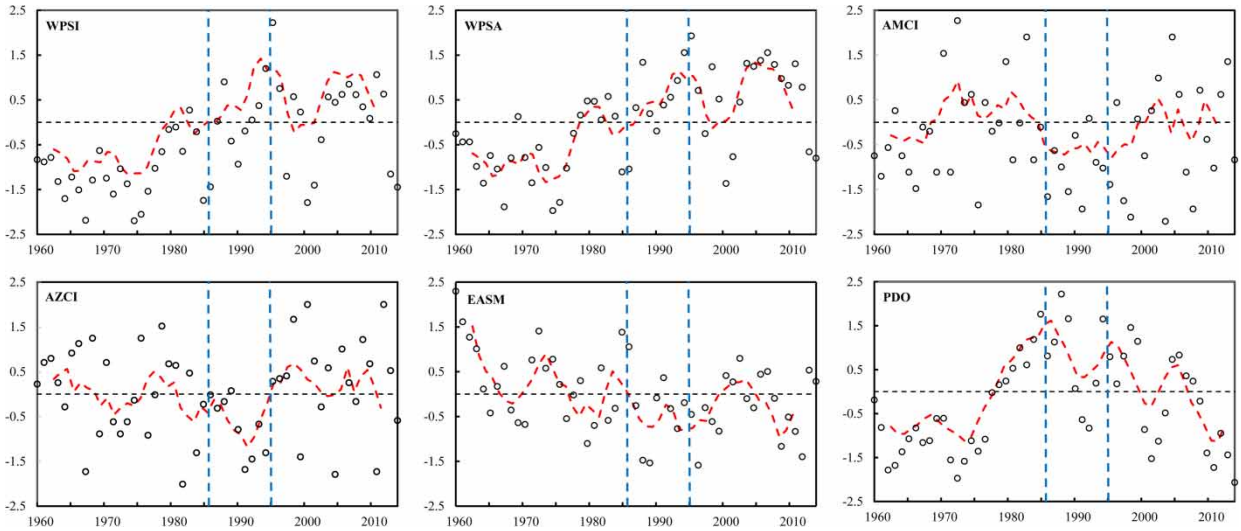

Figure 11 | Mean standardized departures of six atmospheric circulation indexes (WPSI, WPSA, AMCI, AZCI, EASM and PDO) during the 1960–2013 RS. Please refer to the online version of this paper to see this figure in colour: http://dx.doi:10.2166/wcc.2019.250.

conducive to flooding. As shown in Table 6, the AMCI and AZCI are negatively correlated with the SRB-related precipitation index and thus are considered the potential drivers of the precipitation increase in the SRB.

From Period 1 to Period 2, the EASM decreases slightly. According to the characteristics of the EASM, the migration direction of the rain belt in eastern China is determined by the EASM value. When the EASM value is large, the rain belt will migrate to the north. Conversely, the EASM value deviates southward from the rain belt when it is small. However, the EASM usually carries a large amount of water vapour, which may be the reason for the increase in precipitation in the SRB.

The change in the PDO is quite different from the stepwise change of precipitation in the SRB. At the same time, Table 6 shows no significant correlation between the PDO and various precipitation indexes in the SRB, which proves that the PDO has little influence on precipitation in the SRB.

In summary, the meridional and zonal circulation in Asia is considered the potential cause of precipitation and dry/wet changes in the basin. The summer monsoon in East Asia and the western Pacific subtropical high are important factors affecting precipitation and dry/wet changes in the SRB, whereas the PDO has little influence. The results of this study can serve as a reference for studies of the response of cold regions to global climate change and provide a scientific basis for the development of early warning systems for drought in cold regions.

Although we have identified some major atmospheric circulation indices that influence precipitation in the SRB, the amount of precipitation varies greatly from region to region. Precipitation patterns have changed in many areas due to global warming (Mishra & Liu 2014; Ndehedehe *et al.* 2018). Many factors affect precipitation, including not only atmospheric circulation but also temperature (Zhang *et al.* 2013a, 2013b), solar variability (Khare 2012) and different topographies (such as mountains and basins). Different topographies affect the transport of water vapour and thus the formation of precipitation (Cheng *et al.* 2015). Human activity is also a major factor that affects precipitation. Zhu *et al.* (2013) showed that extreme precipitation increased with increasing CO_2 concentrations in southern China. Wan *et al.* (2017) found that precipitation decreased with increasing altitude on the Qinghai–Tibet Plateau. Temperature rises and land cover changes may cause precipitation changes by changing the hydrological cycle and energy budget. Camponogara *et al.* (2014) studied the relationship between biomass burning aerosols in the Amazon and precipitation in the La Plata basin and showed that the concentration of aerosols could inhibit precipitation to some extent. Therefore, the causes of precipitation change in the SRB need to be further explored.

CONCLUSIONS

In this study, the SRB in the mid-high latitudes of Northeast China is selected as the research target. Using statistical methods, the temporal and spatial distributions of the annual and seasonal average precipitation in the SRB and its sub-basins are studied. The SPI is studied using a short-term time scale (SPI3) and a long-term time scale (SPI24) to study the characteristics of regional dry/wet spatial changes and to provide a basis for the rational planning of agricultural production and water resources in the basin. The relationship between monthly precipitation and annual precipitation patterns is also analysed. Finally, atmospheric circulation patterns are considered to analyse the causes of precipitation and dry/wet changes in the SRB. The main findings are summarized as follows:

1. With regard to the spatial distribution, the average annual precipitation decreases to both sides of the high-precipitation belt at 127–129°E. The precipitation in the south-eastern part of the basin is the greatest, and the precipitation in most areas of the basin shows an increasing trend. There is no significant change in the annual precipitation. The spatial distributions of the seasonal precipitation are very similar. The precipitation in the south-eastern part of the basin is greatest, followed by that in the eastern and north-western parts of the basin, whereas the precipitation in the central and south-western parts of the SRB is the lowest. The precipitation in most areas during the spring shows an increasing trend. In most areas, during the summer and autumn, the precipitation shows a decreasing trend. In the winter, the precipitation in the whole basin shows an increasing trend, and the precipitation in most areas increases significantly. These findings can serve as a reference for studying the response of cold regions to global climate change.
2. On a long-term time scale, the south-eastern to the north-western parts of the basin presented a trend of wetness, which alleviated the risk of drought to some extent, whereas other areas presented a trend of dryness. On a short-term time scale, spring presents a trend of wetness, summer and autumn present a trend of dryness, and winter presents a significant trend of wetness. The numbers of moderately and severely dry months have increased significantly in the NRB. These findings can serve as a reference for water resource management and agricultural production in cold regions.
3. Although the average annual precipitation in the SRB shows no obvious trend of change, the annual precipitation shows stepwise changes. The annual precipitation in the SRB and its sub-regions increased from pre-1987 to 1987–2004 and decreased from 1987–2004 to post-2004. Similar stepwise changes are evident in RS precipitation. The average annual precipitation changes are mainly affected by the precipitation changes during the RS (June–August).
4. The precipitation and meteorological wet/dry conditions in the SRB are closely related to several large atmospheric circulation patterns. The meridional and zonal circulation in Asia have been considered as potential causes of precipitation and dry/wet changes in the basin. The western Pacific subtropical high and EASM are also important factors. The results of this study can serve as a reference for studies of the changes in weather patterns in cold regions in response to global climate change and may provide a scientific basis for the development of an early warning system for drought in cold regions.

ACKNOWLEDGEMENTS

This research has been supported by funds from the National Natural Science Foundation of China (51709044 and 51479032) and the National Key R&D Plan (2017YFC0406002).

AUTHOR CONTRIBUTIONS

Tianxiao Li and Zhaoqiang Zhou designed the study. Qiang Fu, Tianxiao Li and Zhaoqiang Zhou wrote the manuscript. Dong Liu, Renjie Hou and Linqi Li performed the data analysis. Qiang Fu, Mo Li and Wei Pei reviewed and approved the manuscript.

COMPETING FINANCIAL INTERESTS

The authors declare no competing financial interest and no non-financial competing interests.

REFERENCES

Abbam, T., Johnson, F. A., Dash, J. & Padmadas, S. S. 2018 Spatiotemporal variations in rainfall and temperature in Ghana over the twentieth century, 1900–2014. *Earth & Space Science* **5** (4), 120–132.

Beamer, J. P., Hill, D. F., Mcgrath, D., Arendt, A. & Kienholz, C. 2017 Hydrologic impacts of changes in climate and glacier extent in the Gulf of Alaska watershed. *Water Resources Research* **53** (9), 7502–7520.

Bordi, I., Fraedrich, K., Jiang, J. M. & Sutera, A. 2004 Spatiotemporal variability of dry and wet periods in eastern China. *Theoretical and Applied Climatology* **79** (1–2), 81–91.

Burn, D. H. & Taleghani, A. 2013 Estimates of changes in design rainfall values for Canada. *Hydrological Processes* **27** (11), 1590–1599.

Camponogara, G., Silva Dias, M. A. F. & Carrió, G. G. 2014 Relationship between Amazon biomass burning aerosols and rainfall over the La Plata Basin. *Atmospheric Chemistry & Physics* **14** (9), 23995–24021.

Cheng, A. F., Feng, Q., Fu, G. B., Zhang, J. K., Li, Z. X., Hu, M. & Wang, G. 2015 Recent changes in precipitation extremes in the Heihe River Basin, Northwest China. *Advances in Atmospheric Sciences* **32** (10), 1391–1406.

Dabanli, I., Mishra, A. K. & Sen, Z. 2017 Long-term spatio-temporal drought variability in Turkey. *Journal of Hydrology* **552**, 779–792.

Dhakal, N. & Tharu, B. 2018 Spatio-temporal trends in daily precipitation extremes and their connection with North Atlantic tropical cyclones for the southeastern United States. *International Journal of Climatology* doi: 10.1002/joc.5535.

Faiz, M. A., Liu, D., Fu, Q., Uzair, M., Khan, M. I., Baig, F., Li, T. X. & Cui, S. 2018 Stream flow variability and drought severity in the Songhua River Basin, Northeast China. *Stochastic Environmental Research & Risk Assessment* **32** (5), 1–18.

Fan, J. J., Huang, Q. & Liu, D. F. 2017 Identification of impacts of climate change and direct human activities on streamflow in Weihe River Basin in Northwest China. *International Journal of Agricultural & Biological Engineering* **10** (4), 119–129.

Feng, B., Zhang, G. X. & Li, F. P. 2016 Characteristics of seasonal meteorological drought and risk regionalization in Songhua River Basin. *Scientia Geographica Sinica* **36** (3), 466–474.

Fu, Q., Li, L. Q., Li, M., Li, T. X., Liu, D. & Zhou, Z. Q. 2018a An interval parameter conditional value-at-risk two-stage stochastic programming model for sustainable regional water allocation under different representative concentration pathways scenarios. *Journal of Hydrology* **564**, 115–124.

Fu, Q., Zhou, Z. Q., Li, T. X., Liu, D., Hou, R. J., Cui, S. & Yan, P. R. 2018b Spatiotemporal characteristics of droughts and floods in northeastern China and their impacts on agriculture. *Stochastic Environmental Research & Risk Assessment* **10**, 1–19.

Gao, L., Huang, J., Chen, X. W., Chen, Y. & Liu, M. B. 2018 Contributions of natural climate changes and human activities to the trend of extreme precipitation. *Atmospheric Research* **205**, 60–69.

Gummadi, S., Rao, K. P. C., Seid, J., Legesse, G., Kadiyala, M. D. M., Takele, R., Amede, T. & Whitbread, A. 2017 Spatio-temporal variability and trends of precipitation and extreme rainfall events in Ethiopia in 1980–2010. *Theoretical and Applied Climatology* **134** (3–4), 1315–1328.

Güner Bacanli, Ü. 2017 Trend analysis of precipitation and drought in the Aegean region, Turkey. *Meteorological Applications* **24** (2), 239–249.

Guo, E. L., Zhang, J. Q., Si, H., Dong, Z. H., Cao, T. H. & Lan, W. 2016 Temporal and spatial characteristics of extreme precipitation events in the Midwest of Jilin Province based on multifractal detrended fluctuation analysis method and copula functions. *Theoretical & Applied Climatology* **130** (1–2), 597–607.

Guo, X. Y., Wu, Z. F., He, H. S., Du, H. B., Wang, L., Yang, Y. & Zhao, W. H. 2017 Variations in the start, end, and length of extreme precipitation period across China. *International Journal of Climatology* **38** (5), 2423–2434.

Guo, H., Bao, A. M., Liu, T., Jiapaer, G., Ndayisada, F., Jiang, L. L., Kurban, A. & Maeyer, P. D. 2018 Spatial and temporal characteristics of droughts in Central Asia during 1966–2015. *Science of the Total Environment* **624**, 1523–1538.

Han, D. M., Yang, G. Y., Yan, D. H. & Fang, H. Y. 2014 Spatial-temporal feature analysis of drought and flood in Northeast China in recently 50 years. *Water Resources and Power* **32** (06), 5–8.

Han, T. T., Chen, H. P. & Wang, H. J. 2015 Recent changes in summer precipitation in Northeast China and the background circulation. *International Journal of Climatology* **35** (14), 4210–4219.

He, X. Z. & Gong, D. Y. 2002 Interdecadal change in Western Pacific subtropical high and climatic effects. *Journal of Geographical Sciences* **57** (2), 185–193.

Huang, J., Sun, S. L., Xue, Y., Li, J. J. & Zhang, J. C. 2014 Spatial and temporal variability of precipitation and dryness/wetness during 1961–2008 in Sichuan Province, West China. *Water Resources Management* **28** (6), 1655–1670.

Huang, J., Xue, Y., Sun, S. L. & Zhang, J. C. 2015 Spatial and temporal variability of drought during 1960–2012 in Inner Mongolia, north China. *Quaternary International* **355**, 134–144. https://doi.org/10.1016/j.quaint.2014.10.036.

Hussain, M. S. & Lee, S. 2014 Long-term variability and changes of the precipitation regime in Pakistan. *Asia-Pacific Journal of Atmospheric Sciences* **50** (3), 271–282.

Jang, C. H., Kim, H. J., Ahn, S. R. & Kim, S. J. 2016 Assessment of hydrological changes in a river basin as affected by climate

change and water management practices, by using the cat model. *Irrigation & Drainage* **65** (S2), 26–35.

Khan, M. I., Liu, D., Fu, Q., Dong, S. H., Liaqat, U. W., Faiz, M. A., Hu, Y. X. & Saddique, Q. 2016 Recent climate trends and drought behavioral assessment based on precipitation and temperature data series in the Songhua River Basin of China. *Water Resources Management* **30** (13), 1–21.

Khare, N. 2012 Indicative proxy evidences of the changing monsoonal precipitation during the last millennium over central west coast of India: a possible link to solar variability. *Oceanology* **52** (4), 495–504.

Lena, B. D., Vergni, L., Antenucci, F., Todisco, F. & Mannocchi, F. 2014 Analysis of drought in the region of Abruzzo (Central Italy) by the standardized precipitation index. *Theoretical and Applied Climatology* **115**, 41–52. https://doi.org/10.1007/s00704-013-0876-2.

Levine, X. J. & Boos, W. R. 2016 A mechanism for the response of the zonally asymmetric subtropical hydrologic cycle to global warming. *Journal of Climate* **29** (21), 7851–7867.

Li, M. & Fu, Q. 2019 An optimal modelling approach for managing agricultural water-energy-food nexus under uncertainty. *Science of the Total Environment* **651**, 1416–1434.

Li, C. & Wang, R. H. 2016 Recent changes of precipitation in Gansu, Northwest China: an index-based analysis. *Theoretical & Applied Climatology* **129** (1–2), 1–16.

Li, X. X., Zhang, X. Z., Zhang, L. J. & Zheng, J. Y. 2017 The varied impacts of land use/cover change on summer precipitation over eastern China. *Geographical Research* **36** (7), 1233–1244 (in Chinese).

Liang, K., Liu, S., Bai, P. & Nie, R. 2015 The Yellow River basin becomes wetter or drier? The case as indicated by mean precipitation and extremes during 1961–2012. *Theoretical & Applied Climatology* **119** (3–4), 701–722.

Liu, W. B., Cai, T. J., Fu, G. B., Zhang, A. J., Liu, C. M. & Yu, H. Z. 2012 The streamflow trend in Tangwang River basin in northeast China and its difference response to climate and land use change in sub-basins. *Environmental Earth Sciences* **69** (1), 51–62.

Lu, Z. H., Xia, Z. Q., Yu, L. L. & Wang, J. C. 2012 Variation of characteristics of annual precipitation and seasonal precipitation in Songhuajiang River Basin. *Hydrology* **32** (02), 62–71. (in Chinese).

Lu, E., Zeng, Y. T., Luo, Y. L., Ding, Y., Zhao, W., Liu, S. Y., Gong, L. Q., Jiang, Y., Jiang, Z. H. & Chen, H. S. 2014a Changes of summer precipitation in China: the dominance of frequency and intensity and linkage with changes in moisture and air temperature. *Journal of Geophysical Research: Atmospheres* **119** (22), 12,575–12,587.

Lu, J. M., Zhu, C., Ju, J. H. & Lin, X. 2014b Interdecadal variability in summer precipitation over East China during the past 100 years and its possible causes. *Chinese Journal of Atmospheric Sciences* **38** (4), 782–794.

Lupikasza, E. 2010 Spatial and temporal variability of extreme precipitation in Poland in the period 1951–2006. *International Journal of Climatology* **30** (7), 991–1007.

McKee, T. B., Doesken, N. J. & Kleist, J. 1993 *The Relationship of Drought Frequency and Duration to Time Scales*. In: *Eighth Conference on Applied Climatology*. American Meteorological Society, Anaheim, CA.

Mehran, A., AghaKouchak, A., Nakhjiri, N., Stewardson, M. J., Peel, M. C., Phillips, T. J., Wada, Y. & Ravalico, J. K. 2017 Compounding impacts of human-induced water stress and climate change on water availability. *Scientific Report* **7** (1), 6282–6290.

Miah, M. G., Abdullah, H. M. & Jeong, C. Y. 2017 Exploring standardized precipitation evapotranspiration index for drought assessment in Bangladesh. *Environmental Monitoring & Assessment* **189** (11), 547.

Miao, J. & Lin, Z. S. 2004 Study on characteristics of the precipitation of nine regions in China and the physical causes. II – The relationship between precipitation and physical causes. *Journal of Tropical Meteorology* **1**, 64–72.

Minaei, M. & Irannezhad, M. 2018 Spatio-temporal trend analysis of precipitation, temperature, and river discharge in the northeast of Iran in recent decades. *Theoretical & Applied Climatology* **131**, 1–13.

Mishra, A. & Liu, S. C. 2014 Changes in precipitation pattern and risk of drought over India in the context of global warming. *Journal of Geophysical Research: Atmospheres* **119** (13), 7833–7841.

Ndehedehe, C. E., Awange, J. L., Agutu, N. O. & Okwuashi, O. W. 2018 Changes in hydro-meteorological conditions over tropical West Africa (1980–2015) and links to global climate. *Global & Planetary Change* **162**, 321–341.

Pakalidou, N. & Karacosta, P. 2017 Study of very long-period extreme precipitation records in Thessaloniki, Greece. *Atmospheric Research* **208**, 106–115.

Paparrizos, S., Schindler, D., Potouridis, S. & Matzarakis, A. 2017 Spatio-temporal analysis of present and future precipitation responses over south Germany. *Journal of Water and Climate Change*, **9** (3), 490–499. jwc2017009.

Peng, X., She, Q. N., Long, L. B., Liu, M., Xu, Q., Zhang, J. X. & Xiang, W. N. 2017 Long-term trend in ground-based air temperature and its responses to atmospheric circulation and anthropogenic activity in the Yangtze River Delta, China. *Atmospheric Research* **195**, 20–30.

Qi, H. X., Zhang, Y. & Cheng, Z. L. 2013 *Floods Caused Direct Economic Losses of 19.1 Billion Yuan in Heilongjiang Province*. Xinhua News Agency Heilongjiang Branch, Harbin (http://hlj.xinhuanet.com/hljpdry/hljpdry.htm).

Raziei, T., Saghafian, B., Paulo, A. A., Pereira, L. S. & Bordi, I. 2009 Spatial patterns and temporal variability of drought in Western Iran. *Water Resources Management* **23** (3), 439–455.

Santos, J. F., Pulido-Calvo, I. & Portela, M. M. 2010 Spatial and temporal variability of droughts in Portugal. *Water Resources Research* **46** (3), 742–750.

Sen, P. K. 1968 Estimates of the regression coefficient based on Kendall's tau. *Journal of the American Statistical Association* **63**, 1379–1389.

Sharma, D. & Babel, M. S. 2014 Trends in extreme rainfall and temperature indices in the western Thailand. *International Journal of Climatology* **34** (7), 2393–2407.

She, D. X., Xia, J., Zhu, L. T., Lv, J. M., Chen, X. D., Zhang, L. P. & Zhang, X. 2016 Changes of rainfall and its possible reasons in the Nansi Lake Basin, China. *Stochastic Environmental Research & Risk Assessment* **30** (4), 1099–1113.

Shi, Z. J., Shan, N., Xu, L. H., Yang, X. H., Gao, J. X., Guo, H., Zhang, X., Song, A. Y. & Dong, L. S. 2016 Spatiotemporal variation of temperature, precipitation and wind trends in a desertification prone region of China from 1960 to 2013. *International Journal of Climatology* **36** (13), 4327–4337.

Shu, S. J., Wang, Y. & Xiong, A. Y. 2007 Estimation and analysis for geographic and orographic influences on precipitation distribution in China. *Chinese Journal of Geophysics* **50** (6), 1703–1712 (in Chinese).

Simonovic, S. P. 2017 Bringing future climatic change into water resources management practice today. *Water Resources Management* **31** (10), 2933–2950.

Song, Y. & Zhao, Y. 2012 Effects of drought on winter wheat yield in north China during 2012–2100. *Acta Meteorologica Sinica* **26**, 516–528.

Song, X., Song, S. B., Sun, W. Y., Mu, X. M., Wang, S. Y., Li, J. Y. & Li, Y. 2015a Recent changes in extreme precipitation and drought over the Songhua river basin, China, during 1960–2013. *Atmospheric Research* **157**, 137–152.

Song, X. Y., Song, S. B., Sun, W. Y., Mu, X. M., Wang, S. Y., Li, J. Y. & Li, Y. 2015b Recent changes in extreme precipitation and drought over the Songhua river basin, China, during 1960–2013. *Atmospheric Research* **157** (157), 137–152.

Ta, Z. J., Yu, R. D., Chen, X., Mu, G. J. & Guo, Y. F. 2018 Analysis of the spatio-temporal patterns of dry and wet conditions in Central Asia. *Atmosphere* **9** (1), 7.

Vergni, L., Lena, B. D., Todisco, F. & Mannocchi, F. 2015 Uncertainty in drought monitoring by the Standardized Precipitation Index: the case study of the Abruzzo region (central Italy). *Theoretical & Applied Climatology* **128** (1), 1–14.

Voisin, N., Hejazi, M., Leung, L. R., Liu, L., Huang, M. Y., Li, H. Y. & Tesfa, T. 2017 Effects of spatially distributed sectoral water management on the redistribution of water resources in an integrated water model. *Water Resources Research* **53** (5), 4253–4270.

Wan, G. N., Yang, M. X., Liu, Z. C., Wang, X. J. & Liang, X. W. 2017 The precipitation variations in the Qinghai-Xizang (Tibetan) Plateau during 1961–2015. *Atmosphere* **8** (5), 80.

Wang, X. Q., Chen, C. S., Zhang, Z. Y. & Shi, D. M. 2006 Regional features of summer drought and flood in Northeast China and corresponding abnormal water-vapor transportation. *Journal of Natural Disasters* **4**, 53–58 (in Chinese).

Wang, Y., Chen, X. & Yan, F. 2015 Spatial and temporal variations of annual precipitation during 1960–2010 in China. *Quaternary International* **380–381**, 5–13.

Wang, Y. F., Xu, Y. P., Lei, C. G., Li, G., Han, L. F., Song, S., Yang, L. & Deng, X. J. 2016a Spatio-temporal characteristics of precipitation and dryness/wetness in Yangtze River Delta, eastern China, during 1960–2012. *Atmospheric Research* **172–173**, 196–205.

Wang, Y. F., Zhang, J. Q., Guo, E. L., Dong, Z. H. & Lai, Q. 2016b Estimation of variability characteristics of regional drought during 1964–2013 in Horqin Sandy Land, China. *Water* **8** (11), 543.

Wei, F. Y. & Huang, J. Y. 2010 A study of downscaling factors atmospheric circulations in the prediction model of summer precipitation in eastern China. *Chinese Journal of Atmospheric Sciences* **34** (01), 202–212 (in Chinese).

Xu, X. D., Lu, C. G., Ding, Y. H., Shi, X. H., Guo, Y. D. & Zhu, W. H. 2013 What is the relationship between China summer precipitation and the change of apparent heat source over the Tibetan Plateau? *Atmospheric Science Letters* **14** (4), 227–234.

Xu, K., Yang, D., Yang, H., Li, Z., Qin, Y. & Shen, Y. 2015 Spatio-temporal variation of drought in China during 1961–2012: a climatic perspective. *Journal of Hydrology* **526**, 253–264.

Zhang, Q., Li, J., Singh, V. P. & Xu, C. Y. 2013a Copula-based spatio-temporal patterns of precipitation extremes in China. *International Journal of Climatology* **33** (5), 1140–1152.

Zhang, Q., Li, J. F., Singh, V. P. & Xiao, M. Z. 2013b Spatio-temporal relations between temperature and precipitation regimes: implications for temperature-induced changes in the hydrological cycle. *Global & Planetary Change* **111** (4), 57–76.

Zhang, D. D., Yan, D. H., Wang, Y. C., Fan, L. & Wu, D. 2015 Changes in extreme precipitation in the Huang-Huai-Hai River basin of China during 1960–2010. *Theoretical & Applied Climatology* **120** (1–2), 195–209.

Zhao, G. J., Mu, X. M., Hormann, G., Fohrer, N., Xiong, M., Su, B. D. & Li, X. C. 2012a Spatial patterns and temporal variability of dryness/wetness in the Yangtze River Basin, China. *Quaternary International* **282**, 5–13. https://doi.org/10.1016/j.quaint.2011.10.020.

Zhao, J. H., Feng, G. L., Yang, J., Zhi, R. & Wang, Q. G. 2012b Analysis of the distribution of the large-scale drought/flood of summer in China under different type of the western Pacific subtropical high. *Acta Meteorologica Sinica* **70** (05), 1021–1031.

Zheng, Y. H., He, Y. & Chen, X. 2017 Spatiotemporal pattern of precipitation concentration and its possible causes in the Pearl River basin, China. *Journal of Cleaner Production* **161**, 1020–1031.

Zhong, K. Y., Zheng, F. L., Wu, H. Y., Qin, C. & Xu, X. M. 2017 Dynamic changes in temperature extremes and their association with atmospheric circulation patterns in the Songhua River Basin, China. *Atmospheric Research* **190**, 77–88.

Zhu, J., Huang, D. Q., Zhou, P. & Lin, H. J. 2013 Simulating the response of non-uniformity of precipitation extremes over China to CO_2, increasing by MIROC-Hires model. *Journal of Tropical Meteorology* **19** (4), 331–339.

First received 22 October 2018; accepted in revised form 5 March 2019. Available online 25 April 2019